ORIGINAL ARTICLE

Sapphirine granulites from Panasapattu, Eastern Ghats belt, India: Ultrahigh-temperature metamorphism in a Proterozoic convergent plate margin

C.V. Dharma Rao [a,*], M. Santosh [b], Reia M. Chmielowski [c]

[a] *National Disaster Management Authority, Government of India, A-1 Safdarjung Enclave, New Delhi, India*
[b] *Department of Interdisciplinary Science, Faculty of Science, Kochi University, Akebono-cho, Kochi 780-8520, Japan*
[c] *Dipartimento di Scienze della Terra, Università degli Studi di Milano, Italy*

Abstract We report equilibrium sapphirine + quartz assemblage in biotite−orthopyroxene−garnet granulites from a new locality in Panasapattu of Paderu region in the Eastern Ghats granulite belt, which provide new evidence for ultrahigh-temperature (UHT) metamorphism at 1030−1050 °C and 10 kbar in this region. The development of migmatitic texture, stabilization of the garnet−orthopyroxene− plagioclase−K-feldspar association, prograde biotite inclusions within garnet and sapphirine as well as sapphirine and cordierite inclusions within garnet in these granulites indicate that the observed peak assemblages probably formed during prograde dehydration melting of a Bt−Sill−Qtz assemblage, and constrain the prograde stage of the p−T path. The core domains of orthopyroxene porphyroblasts have up to $w(Al_2O_3)$ 9.6%, which suggest that the temperatures reached up to 1150 °C suggesting extreme crustal metamorphism. These conditions were also confirmed by the garnet−orthopyroxene thermobar- ometry, which yields a p−T range of 1012−960 °C and 9.4 kbar. The p−T phase topologies computed using isochemical sections calculated in the model system Na_2O−CaO−K_2O−FeO−MgO−Al_2O_3−SiO_2 −H_2O (NCKFMASH) for metapelites, garnet-free sapphirine granulites and garnet-bearing sapphirine granulites match the melt-bearing assemblages observed in these rocks. Isochemical sections constructed

in the NCKFMASH system for an average sub-aluminous metapelite bulk composition, and contoured for modal proportions of melt and garnet, as well as for the compositional isopleths of garnet, predict phase and reaction relations that are consistent with those observed in the rocks. Garnet and orthopyroxene contain Ti-rich phlogopite inclusions, suggesting formation by prograde melting reactions at the expense of phlogopite during ultrahigh-temperature conditions. These $p-T$ results underestimate 'peak' conditions, in part as a result of the modification of garnet compositions in the domains where some melt was retained. The post-peak evolution is constrained by a succession of melt-present reactions that occur at $p < 10$ kbar, inferred from micro-structural relations among various minerals. After high-temperature decompression from the metamorphic peak, the $p-T$ path followed a near isobaric cooling stage to $T < 900\ °C$. The UHT rocks investigated in this study occur within a continental collision suture which witnessed prolonged subduction–accretion history prior to the final collision. We correlate the extreme metamorphism and the stabilization of UHT mineral assemblages to heat and volatile input from an upwelled asthenosphere during subduction–collision tectonics in a Proterozoic convergent plate margin.

1. Introduction

Ultrahigh-temperature (UHT) metamorphism (900–1100 °C, 7–13 kbar) of the continental crust (Harley, 1998a; Kelsey, 2008) has recently been recognized as a common phenomenon in orogenic belts developed along continental collision zones, particularly where subduction-collision tectonics associated with the amalgamation of supercontinent assemblies provided heat and volatile input to stabilize the UHT mineral assemblages (e.g., Santosh et al., 2007; Santosh and Kusky, 2010). The UHT conditions of granulite facies metamorphism, which may be quantified using calculated phase diagram methods, are usually preserved in volumetrically rare high Mg–Al sapphirine granulites with characteristic mineral associations such as sapphirine + quartz, and sillimanite + orthopyroxene (e.g., Harley, 1998b, 2008; Brown, 2007; Kelsey, 2008; Santosh et al., 2007, 2009b; Nishimiya et al., 2010, among others). Sapphirine-bearing UHT granulites have been widely reported from the Eastern Ghats granulite belt where the paragenetic features, reaction textures and $p-T$ evolution have been well documented in previous studies (e.g., Lal et al., 1987; Mohan et al., 1997; Sengupta et al., 1997; Dharma Rao and Chmielowski, 2010, etc.). However, the evidence for a stable coexistence of Spr + Qtz, one of the diagnostic features of UHT rocks (e.g., Harley, 2008; Kelsey, 2008), has not been convincingly demonstrated from this region. Moreover, opinions are sharply divided on the $p-T-t$ paths inferred from the Mg–Al sapphirine granulites in the Paderu area. Lal et al. (1987) had earlier suggested a clockwise path with decompression following the UHT peak condition for these rocks. However, Pal and Bose (1997) and Sengupta et al. (1997) reinterpreted the petrographic data of Lal et al. (1987) to propose a general anticlockwise path. In their study, the prograde path reached a peak of $p = 9.5$ kbar, $T = \sim1000\ °C$ and was followed by near isobaric cooling to $p = 9$ kbar, $T = 900\ °C$. Bhattacharya and Kar (2002) and Bhattacharya et al. (2003) also proposed a clockwise path from the Paderu region, in which peak $p-T$ conditions of ~10 kbar and $\sim1000\ °C$ were followed by high-temperature decompression and subsequent isobaric cooling. However, as pointed out by Sengupta et al. (2004), their study is afflicted by inconsistencies in the documentation and petrologic interpretation of reaction textures with serious errors in the thermodynamic evaluation. Sengupta et al. (2004) suggested that the data are more consistent with decompression from a lower pressure of 7–8 kbar and $T = 850\ °C$. This decompression post-dated the cooling from the UHT

conditions. The pattern would thus be similar to the anticlockwise pattern in other areas in EGB, as well as those reported for sapphirine-bearing UHT granulites from other regions (e.g., Santosh et al., 2007, 2009b).

In this contribution, we provide robust evidence for the stable coexistence of Spr + Qtz in the UHT granulites of Paderu. Furthermore, both inverse methods (e.g., thermobarometry) and forward modeling (isochemical sections) of well-constrained micro-structural relations and mineral assemblages are used to investigate, in a quantitative manner, the metamorphic evolution of high-grade subsolidus and suprasolidus (migmatitic) metapelitic rocks and associated sapphirine granulites in a previously uninvestigated region of Panasapattu UHT locality in Paderu. The isochemical sections have been calculated in the model system Na₂O–CaO–K₂O–FeO–MgO–Al₂O₃–SiO₂–H₂O (NCKFMASH). Several recent studies have demonstrated the potential of the application of isochemical sections ("pseudosections") to evaluate the stability of mineral assemblages and their evolution in $p-T$ space during prograde, peak and retrograde metamorphism (e.g., Tinkham et al., 2001; White et al., 2001; White and Powell, 2002; Zeh and Holness, 2003; Kelsey, 2008; Nasipuri et al., 2009; Dharma Rao and Chmielowski, 2010). The results in this study thus provide new insights on UHT conditions in a deeply buried crustal segment of the Eastern Ghats belt with implications for the thermal and tectonic evolution of this collisional orogen.

2. Geological and tectonic background

Recent studies provide increasing evidence that the south-eastern margin of the Indian continental fragment (Fig. 1) underwent extensive rifting events during the Paleoproterozoic (e.g., French et al., 2008) associated with the global disintegration of the Columbia supercontinent (Rogers and Santosh, 2002, 2009). The Paleo-Mesoproterozoic rifting developed a passive margin along the eastern periphery of the Indian proto-continent, and enlarged into an ocean which opened toward southeast. The initiation of the closing phase of the ocean floor, its subduction and imbrication at the eastern periphery of the Archean Dharwar craton are recorded from recent studies of ophiolitic assemblages from Kanigiri (Dharma Rao and Reddy, 2009; Dharma Rao et al., 2011b) which provide U-Pb ages of ~1.33 Ma from zircons in gabbros and plagiogranites. The subduction associated with the closure of a wide ocean would also create a series of accretionary complexes,
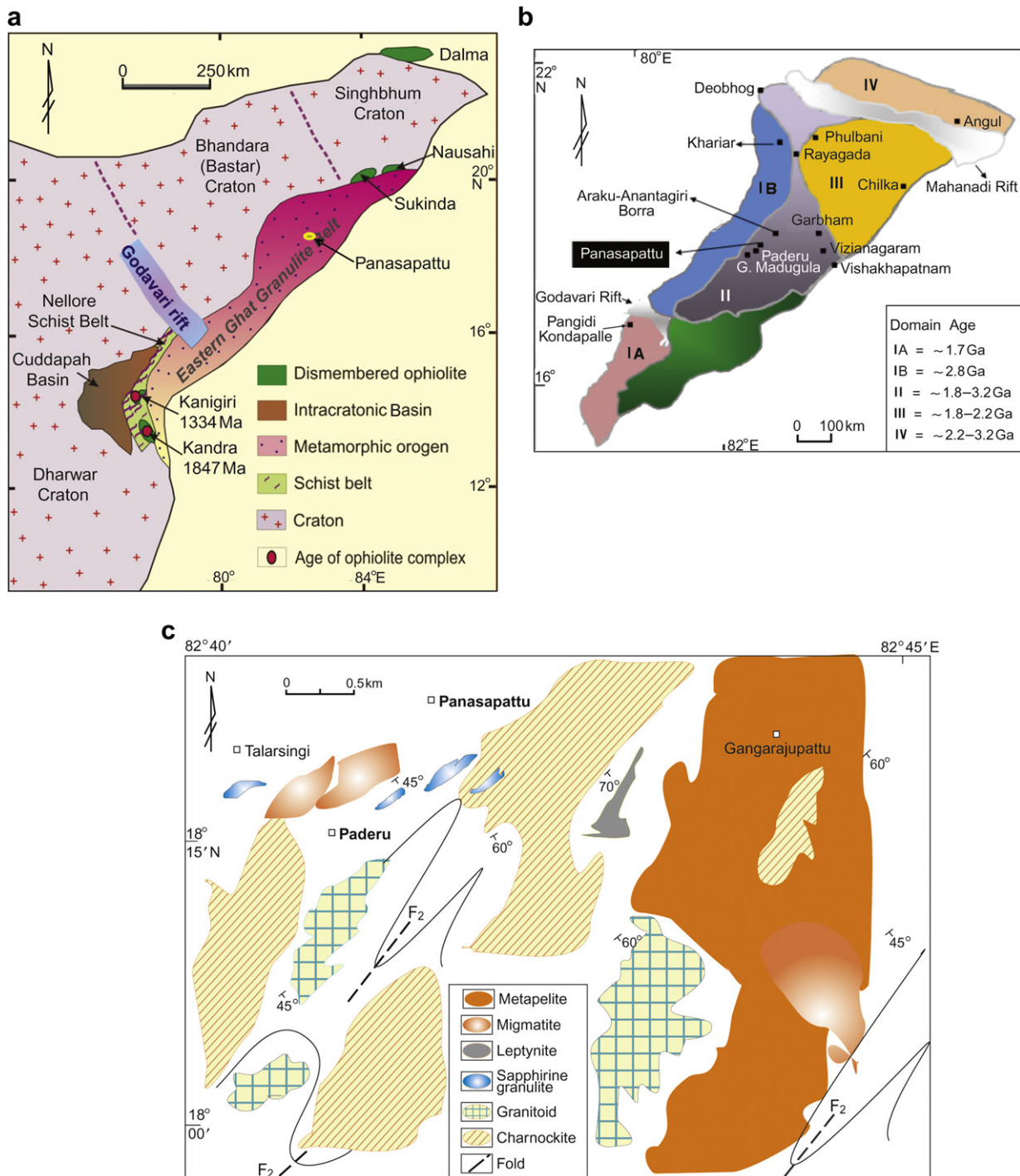
Figure 1   a: Map showing various cratons along with major litho-tectonic subdivisions of the Peninsular India. The map shows location of the present study area. Distribution of rocks considered to represent fragments of dismembered ophiolites at the sutured margins along the craton-mobile belt contact are also shown (map modified from Dharma Rao et al., 2010). b: Map of the Eastern Ghats belt showing various domains based on isotopic data of Rickers et al. (2001) and the location of Panasapattu. c: Simplified geological sketch map of Panasapattu study area showing major rock types.

and if subduction of a mid-oceanic ridge was involved, high temperature and high pressure regional metamorphic belts would also be generated (e.g., Santosh and Kusky, 2010). The Protero-zoic Eastern Ghats belt that extends over 1000 km from the Brahmani river valley in Orissa to south-eastern parts of Andhra Pradesh along the eastern coast of the Indian peninsula record

tectono-metamorphic events ranging in age from Mesoproterozoic to Neoproterozoic and incorporates a wide 'khondalite belt' of metamorphosed passive margin sequence, in association with arc magmatic rocks and remnants of metamorphosed oceanic crust in the form of high pressure mafic granulites, similar to the Paleo-proterozoic khondalite belt in the North China Craton (e.g.,

Santosh, 2010; Santosh et al., 2010). The Eastern Ghats belt also preserves evidence for regional-scale anomalous extreme thermal conditions of metamorphism in excess of 1000 °C at lower crustal pressure of 8–10 kbar (Dasgupta and Sengupta, 2003). The western margin of the Eastern Ghats belt, where the granulites are thrust over cratonic rocks, is widely considered as a collision suture (Dobmeier and Raith, 2003), and several studies have documented evidence for high-grade metamorphism, magmatism and deformation at various intervals during the Meso- and Neoproterozoic time (see reviews by Dobmeier and Raith, 2003; Simmat and Raith, 2008; Mukhopadhyay and Basak, 2009). In a previous study, Dobmeier and Raith (2003) proposed several crustal provinces within this belt, although the temporal and tectonic relations among these provinces have not been well constrained (Mukhopadhyay and Basak, 2009). The inclusion of units with contrasting metamorphic grade and structural style within the different provinces has also been questioned (Gupta, 2004).

One of the notable features of the Eastern Ghats belt is the occurrence of arc magmatic rocks together with high p–T metamorphic rocks, probably exposing the root zone of a subduction system (Dharma Rao and Reddy, 2009; Dharma Rao et al., 2010; Dharma Rao and Santosh, 2011; Dharma Rao et al., 2011a, b). Recent reports of ophiolitic rocks (Fig. 1a) from the margin of this collisional belt with the Archean Dharwar craton to the west (Dharma Rao et al., 2011b; Saha, 2011) suggest a prolonged subduction and accretion process prior to the final collision in the Neoproterozoic, probably coinciding with the Rodinia supercontinent assembly. The Eastern Ghats belt is thus the trace of the Rodinia collisional suture and recent geochronological studies based on more precise techniques identify the timing of UHT metamorphism in this belt to range from 1.63 Ga (Upadhyay et al., 2009) to ca. 1.0 Ga (Das et al., 2010). Ages in between this range have also been reported from different sectors, which probably suggest an episodic exhumation of high p–T metamorphic orogens within a subduction–accretion regime as reported from the Cambrian collisional suture in southern India (Santosh et al., 2009a), and comparable with an identical scenario in the Pacific-type orogenic belts in Japan (e.g., Isozaki et al., 2010). The formation of extreme metamorphic rocks in such tectonic settings has also been correlated to asthenospheric upwelling through slab window opening during episodes of ridge subduction (e.g., Santosh and Kusky, 2010). The present study area is located near the village of Panasapattu (latitude 18°0′ N–18°16′ N and longitude 82°40′ E–82°45′ E) about 2 km northeast of the Paderu town in Visakhapatnam district of Andhra Pradesh (18°04′ N; 82°38′ E) in the southern sector of the Eastern Ghats belt (Fig. 1a and b).

3. Outcrop setting and petrography

Fig. 1c is a generalized geological map of the study area. The dominant rock types exposed in the area are metapelitic granulites, enclaves of mafic granulites, charnockites and their variants, and granitoids. The mafic granulites and granitoids are volumetrically less abundant as compared to the metapelites. The metapelitic rocks can be divided into three compositional groups based on their mineral assemblages and distinct bulk compositions, namely, aluminous granulites, leptynites (with restite streaks), and high Mg–Al sapphirine granulites. The sapphirine granulites form two sub-groups: garnet-bearing and garnet-free. The structural history of these rocks provides evidence for multiple deformation

(F_1, F_2 and F_3). The F_2 folds observed on various scales determine the overall antiformal structural pattern. Evidence for F_2 deformation on a mesoscopic scale includes: pre- to syn- F_2 leucosomes bands in migmatized metapelitic granulites and leucocratic "melt" layers in granitoids. Almost regularly spaced foliation-parallel leucosomes with garnet poikiloblasts alternating with melanosomes that represent "in situ" melt segregation are also present. The migmatites show layer-parallel leucosomes with thicker melanosomes, suggesting formation by grain-scale flow of melt from less competent to more competent layers. The large ovoid peritectic garnet poikiloblasts scattered throughout the matrix of migmatite within strongly foliated sillimanite–biotite-rich host are inferred to record melt loss pathways.

The high Mg–Al sapphirine granulites occur as layers within massive charnockites and granites and as folded bands (or layers) probably suggesting their imbrication within arc magmatic units (Fig. 2a). The F_1 folds are quartzite bands (Fig. 2b) in metapelites. Large scale F_2 folds are commonly overturned with steep plunges. The F_3 folds have E–W axial traces. An S_1 granulite-facies banding is defined by alternate aluminous layers (rich in porphyroblastic garnet and sillimanite) and K-feldspar–quartz ± plagioclase leucosomes in common metapelitic granulites and streaky gneissic foliation in the charnockites. The restite streaks in leptynite are inter-layered with metapelites. A summary of mineral assemblages along with melt related microstructural features of each rock type is given in Table 1. The
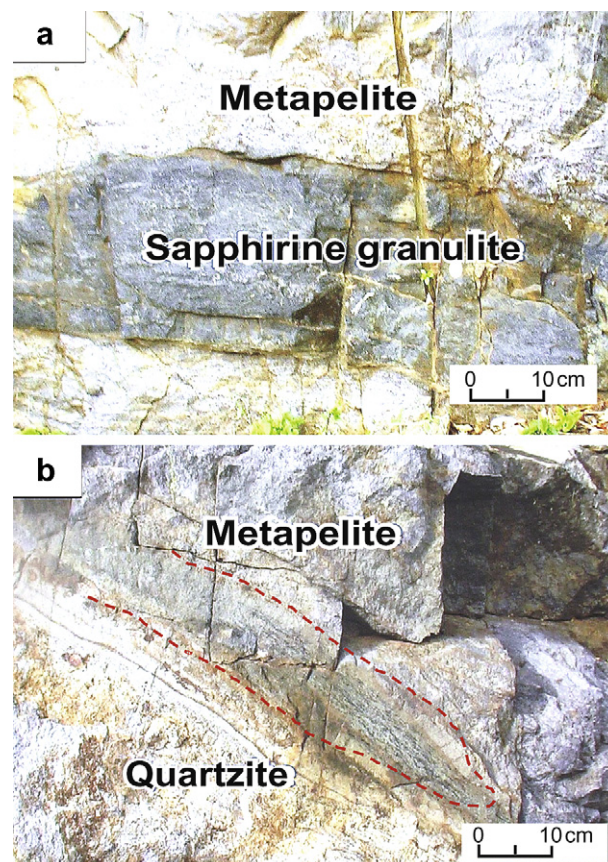
Figure 2 Outcrop photographs of UHT rocks of Panasapattu area. a: Sapphirine granulite band in khondalite representing F_1 folds; b: Quartzite bands in khondalite representing F_1 folds. Dashed line indicates the trace of the fold.

mineral abbreviations in this paper are after Whitney and Evans (2010).

3.1. Metapelitic granulites (khondalite) (TK-12)

The metapelitic granulites are of two types. The first type granulites possess a pronounced foliation, often accentuated by layer-parallel leucosomes. The second type, while broadly similar in composition, is migmatitic with leucosomes occurring as bands alternating with melanosome consisting of megacrystic garnet and biotite. The most common rock type in the study area is the metapelitic granulite, locally known as khondalite, with an assemblage of Grt−Kfs−Qtz−Bt−Sill, suggesting an aluminous sedimentary protolith. Minor amounts of K-feldspar and plagioclase (An_{68}) are present as accessories. The rock is locally extremely deformed, producing pervasive gneissic S_2 foliation defined by sub-parallel sillimanite blades within the quartzo-felspathic matrix (Fig. 3a, b). Lecucocratic domains defined by quartzo-felspathic segregations and melanaocratic domains containing garnet and biotite are present. Small (<1 cm) quartz−feldspar patches are oriented parallel to the sillimanite relics (Fig. 3b). Some leucocratic domains show bimodal distribution based on grain size. Thus, large K-feldspar (perthite) grains are set in finer grained bands of quartz and plagioclase (Fig. 3c) separated by discrete layers of biotite (Fig. 3c). Small plagioclase + K-feldspar grains embay relict K-feldspar grains (Fig. 3c) and a biotite-rich selvage is present in the fringe of K-feldspar−quartz rich domains (Fig. 3c). The leucocratic portions in some domains exhibit melt pools defined by inclusion filled oikocrystic quartz enclosing highly cuspate plagioclase grains (Fig. 3d) that probably grew directly from the melt. In melanaocratic domains inclusion-poor cuspate porphyroblast garnet contains few small rounded inclusions of quartz (Fig. 3e). Late biotite−quartz intergrowths and patchy K-feldspar intergrowths occur along garnet margins. A pervasive S_2 foliation is defined by oriented biotite wraps around garnet (Fig. 3f).

3.2. Migmatite (TK-10)

Migmatitic metapelitic gneisses have the assemblage Grt−Pl−Kfs−Qtz−Bt. They have alternate layers of melanosome (rich in porphyroblastic garnet and, biotite, and containing rare sillimanite) and leucosomes (K-feldspar−quartz ± plagioclase). The centimeter-scale leucosomes carry different proportions of granular aggregates of megacrystic plagioclase, K-feldspar and quartz. The K-feldspar forms completely recrystallized aggregates (0.2−0.8 mm grain size) with straight grain boundaries locally meeting in triple point junctions at 120°. Plagioclase is present in K-feldspar aggregates as small interstitial grains or forms thin films preferentially tracing those of K-feldspar. The plagioclase grains show common twinning and exhibit normal zoning. The intensity of quartz and plagioclase lobes commonly correlates well with highly cuspate irregular forms of corroded relics of K-feldspar. Crosscutting micro-veins are filled by biotite. Porphyroblast garnet with rounded cuspate boundaries occurs in the melanosomes layers. Rare sillimanite relics also occur in the melanosomes. The plagioclase present in some of the samples indicates the presence of greywacke-like protolith, unlike the typical khondalites of other areas in the Eastern Ghats belt (cf. Dharma Rao, 1998, 2000; Sengupta et al., 1999). The absence of prograde biotite in host khondalite suggest their restitic nature and the occasional presence of quartzo-felspathic pods may be a product of partial melting from which a partial melt had presumably been extracted.

3.3. Leptynite gneiss (P-51b)

The restite streaks of leptynite gneiss have a similar mineral assemblage to the metapelitic granulites, although sillimanite is absent as a matrix mineral indicating a less aluminous bulk composition. The rock is locally intensely deformed, producing gneissic foliation (S_2) which envelopes garnet porphyroblasts. A pervasive S_2 foliation defined by crudely oriented biotite wraps around lozenge-shaped garnet. Elongate quartz + K-feldspar ribbons define a distinctive, leptynitic foliation. Quartz ribbons (0.3−1.0 mm in width) are composed of elongate grains with straight grain boundaries perpendicular to the ribbon margin. Porphyroblast garnet (20%−30% by mode) contains a folded internal schistocity, S_1 is defined by relict laths of sillimanite. Biotite and quartz are also included in the garnet. Large inclusion-free garnets with elongate quartz ribbons are also replaced extensively by large biotite laths and small quartz grains along the garnet margins. Bulbous myrmekite and highly irregular lobate grains that overgrow partially resorbed corroded plagioclase

Table 1 Mineral assemblages, melt features and chemical data of Panasapattu rocks. All numbers refer to x_{Mg}, except Al_2O_3 for Opx and x_{An} for plagioclase.

Sample	Assemblage	Melt features	Grt	Opx	Al₂O₃	Spr	Bt	Crd	Pl
TK-12	Grt−Kfs−Qtz−Bt	Qtz−Kfs patches Melt pools Myrmekite Cuspate garnet	0.47				0.77		0.68
TK-10	Grt−Pl−Kfs−Qtz−Bt	Melt films of Pl on Kfs Cuspate Kfs Melt-pseudomorphs of Kfs Shape of Qtz mimic former melt	0.59				0.86		0.51
P-51b	Grt−Kfs−Qtz−Bt−Pl	Bulbous myrmekite	0.41				0.81		0.69
P-63	Spr−Opx−Crd			0.68	9.86	0.78		0.9	
P-60	Spr−Qtz−Opx−Crd−Kfs	Pl−Kfs dihedral angles		0.77	8.66	0.80	0.81	0.87	0.51
P-62	Spr−Qtz−Opx−Crd−Bt−Spl−Pl−Kfs	Pl film on Kfs		0.72	8.78	0.90	0.89	0.89	0.44
P-61a	Grt−Bt−Opx−Sil−Spr−Crd−Qtz	Euhedral Grt	0.46	0.78	7.65	0.78	0.89	0.92	
P-61b	Grt−Bt−Opx−Spr−Crd−Qtz	Euhedral Grt	0.60	0.70	8.78	0.75	0.89		
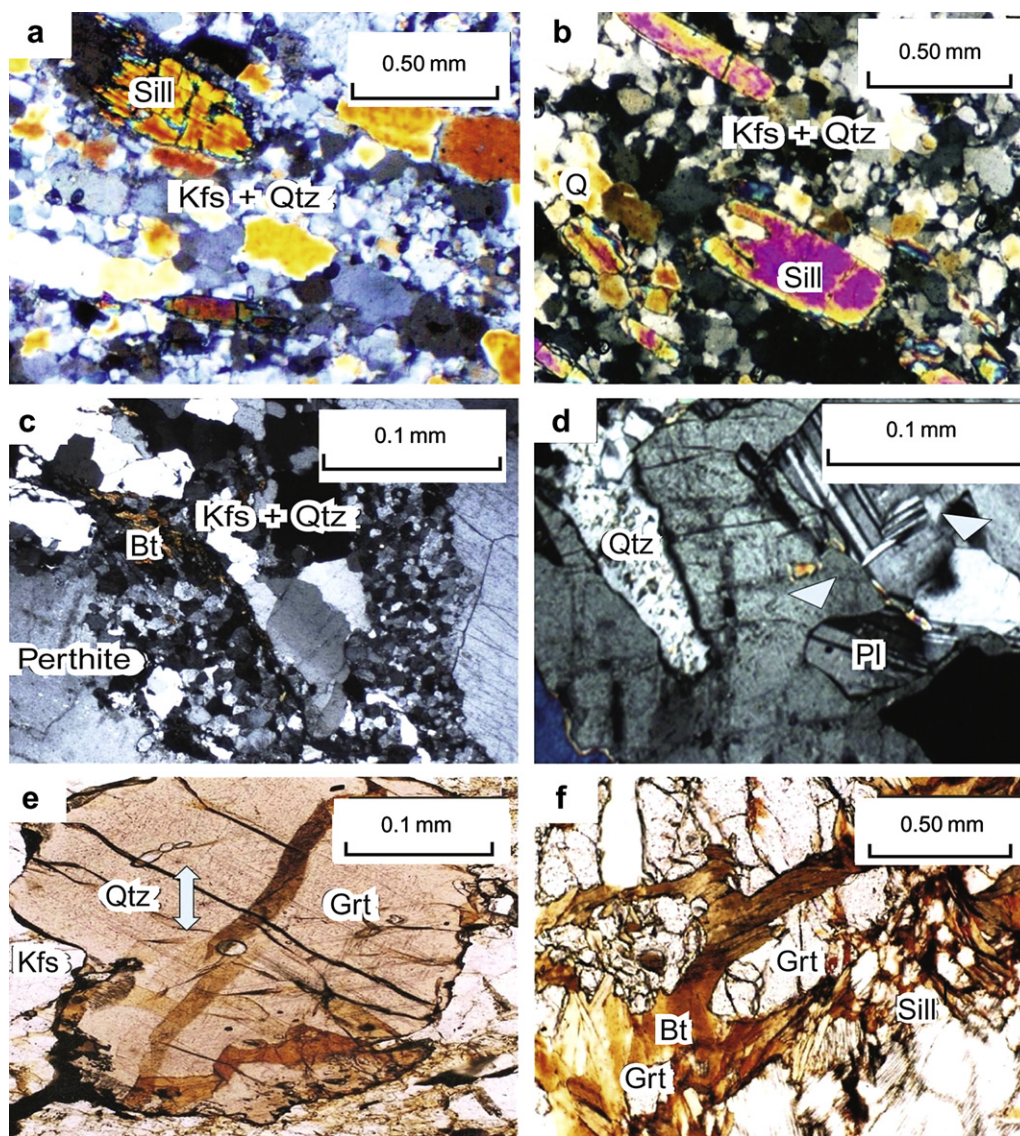
Figure 3   a: Crossed polarized light photomicrograph of pervasive gneissic S_2 foliation defined by oriented sillimanite lathes and elongated ribbon quartz in a foliated SE−NW oriented the quartzo-felspathic matrix; b: Crossed polarized light photomicrograph showing oriented silli-manite relics in foliated quartzo-felspathic matrix. Note the small (<1 cm) quartz−feldspar patches oriented almost parallel to the foliation; c: Crossed polarized light image of large K-feldspar (perthite) set in a matrix of finer grained bands of quartz and feldspars separated by selvage of biotite. Note the bimodal distribution of mineral sizes; d: Crossed polarized light image of melt pool defined by inclusion filled oikocrystic quartz and enclosing highly cuspate feldspar grains crystals enclosed in large K-feldspar grain in the leucocratic portions of the rock; e: Cuspate shaped inclusion-poor porphyroblast garnet contain with tiny blebs of small quartz inclusions in melanaocratic domains of the rock; f: Oriented biotite wraps around elongated inclusion-free garnet defining a pervasive S_2 foliation. Biotite−quartz intergrowths and patchy K-feldspar intergrowths occur along garnet margins. Biotite also occurs as inclusions within sub-hedral garnet.

grains occur in the leucocratic domains. Sillimanite laths and biotite inclusions within some garnets suggest a psammo-pelitic intercalation of the protoliths of leptynites.

3.4. High Mg−Al sapphirine granulites

In the Panasapattu area, the garnet-free sapphirine granulites can be further divided into a fine-grained and a coarse-grained category. In the fine-grained variety (e.g., sample P-63), the charac-teristic assemblage is Spr−Opx−Crd. Minor amounts of biotite, sillimanite and quartz also occur. These rocks show a weakly

foliated microstructure with a grain size that varies from 5 to 50 mm. Biotite occurs as weakly oriented grains along with sapphirine and cordierite (Fig. 4a). The coarse-grained variety (e.g., samples P-60, 62) shows an assemblage Spr−Qtz−Opx−Crd−Kfs. Biotite, plagioclase and spinel occur in minor amounts. They are migmatitic with plagioclase and K-feldspar in quartzo-felspathic segregations imparting the migmatitic structure. The plagioclase and K-feldspar exhibit dihedral angles. Quartz and orthopyroxene are absent in the melanocratic layers. Sapphirine in mutual contact with quartz occurs as stumpy grains with inclu-sions of spinel. Sapphirine and biotite define the main foliation of
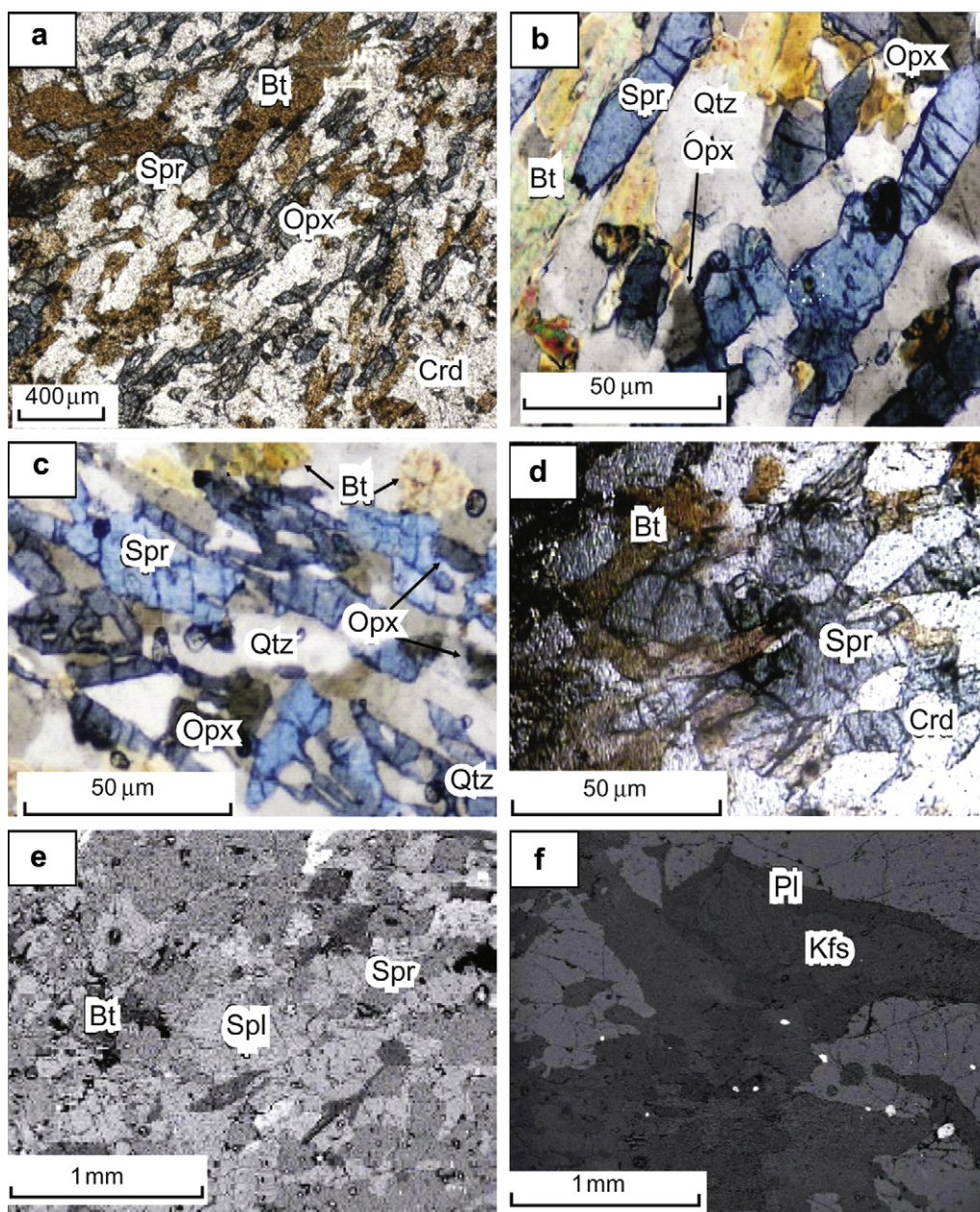
Figure 4 a: Crossed polarized light image of granular aggregates of sapphirine–orthopyroxene–biotite in a weakly foliated microstructure; b: Crossed polarized light photomicrograph of stumpy sapphirine grains defining a foliation. Sapphirine (blue) is seen in mutual contact with quartz (white) along with orthopyroxene and biotite; c: Crossed polarized light photomicrograph of coarse grains of sapphirine along with orthopyroxene and biotite; d: Crossed polarized light photomicrograph of coexisting coarse sapphirine and quartz along with orthopyroxene and cordierite; e: Crossed polarized light photomicrograph of aggregates of sapphirine biotite and rare porphyroblastic spinel occurs in irregular patches throughout leucocratic layers in the rock; f: BSE image of rim of plagioclase on the K-feldspar grain.

the rock (Fig. 4b and c). Sapphirine also occurs as coarse grains along with orthopyroxene (Fig. 4c).

Sample P-62 has the assemblage Spr–Qtz–Opx–Crd–Bt–Spl–Pl–Kfs. This sample is similar to the characteristic assemblage reported in high Mg–Al metapelites (type P–II) from Paderu by Bhattacharya and Kar (2002). Sapphirine in mutual contact with quartz occurs as coarse grains along with Crd and biotite (Fig. 4d). Aggregates of porphyroblastic spinel (Fig. 4e) occur in irregular patches throughout leucocratic layers in the

rock. Small euhedral garnets are associated with the biotite. Plagioclase forms complex intergrowths with quartz. The most characteristic feature in the leucocratic layers is the presence of films of plagioclase on the K-feldspar grains (Fig. 4f). The garnet-bearing sapphirine granulites in the study area show wide variations in grain size at thin section scale. They are divided into two types of assemblages.

Assemblage I (e.g., sample P-61a) shows Grt–Bt–Opx–Sill–Spr–Crd–Qtz. K-feldspar plagioclase, garnet, biotite and

apatite occur in accessory amounts. A S_1 granulite-facies banding is defined by alternate aluminous layers (rich in porphyroblastic orthopyroxene and sillimanite) and K-feldspar–quartz ± plagioclase leucosomes. Sapphirine is rare and occurs within garnet as elongate inclusions together with quartz (Fig. 5a). Orthopyroxene occurs as coarse grains along with sillimanite and cordierite in melanocratic portions of the rock (Fig. 5b). Meso-perthite is commonly observed in leucocratic domains. Biotite in equilibrium with sapphirine is randomly oriented between sapphirine and garnet layers (Fig. 5c). A partial rim of biotite

occurs along resorbed porphyroblastic garnet boundaries with few small grains of sapphirine (Fig. 5d). Garnet occurs as porphyro-blasts and contains sapphirine–orthopyroxene symplectites rim-med by cordierite at its margins. Cordierite occurs as corona on sapphirine–orthopyroxene symplectites (Fig. 5d–f). Small euhe-dral garnets occur between the symplectites (Fig. 5d–f).

Assemblage II (sample P–61b) differs from assemblage I in the absence of sillimanite. The sapphirine and biotite in this rock occur in a foliated microstructure within porphyroblast garnet (Fig. 6a). Sapphirine + quartz also occur within porphyroblast garnet (Fig. 6b).
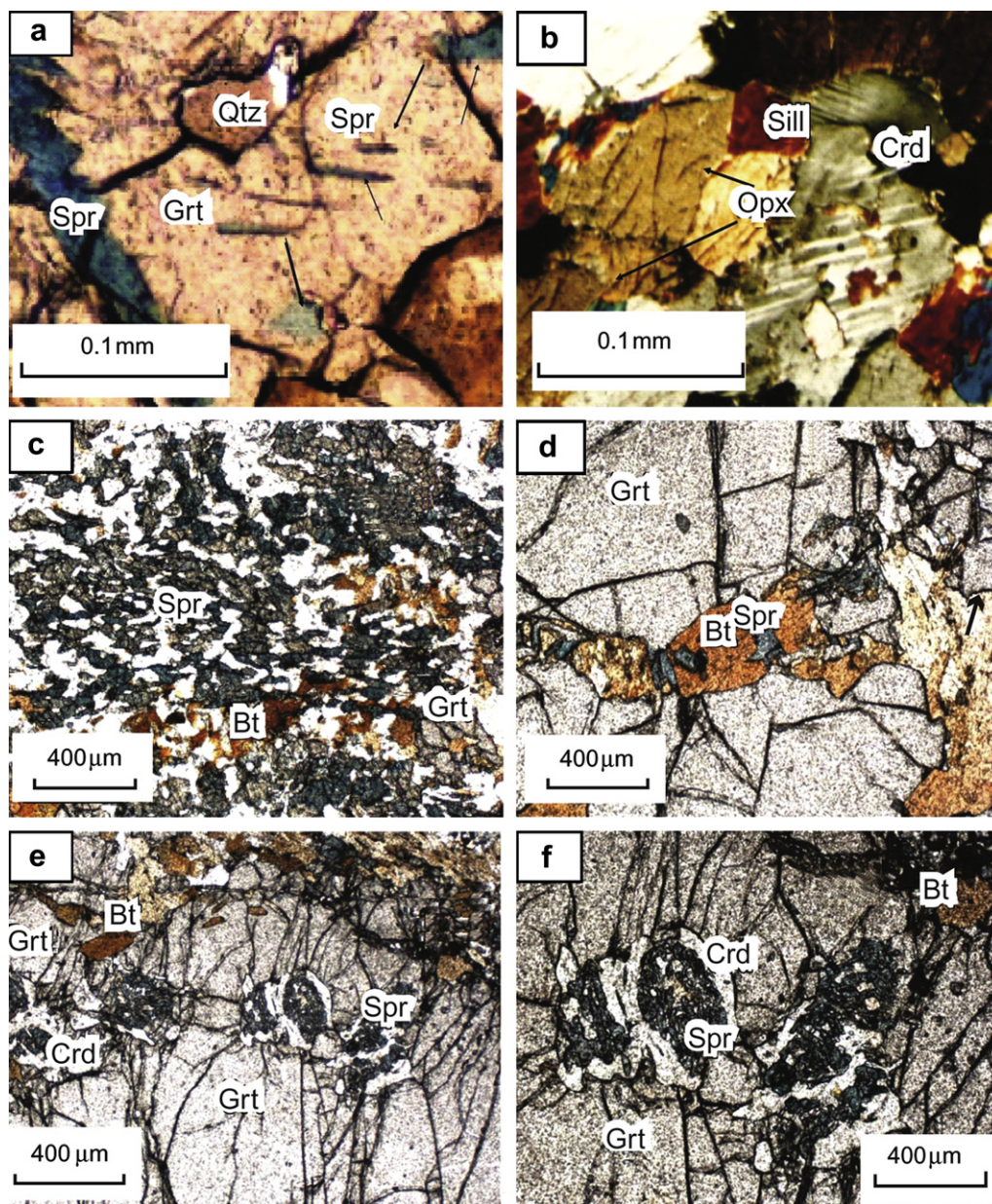
Figure 5   a: Crossed polarized light photomicrograph of sapphirine occurring in garnet as rib-like inclusions along with quartz; b: Crossed polarized light photomicrograph of coarse-grained orthopyroxene along with sillimanite and cordierite in melanocratic portions of the rock; c: Crossed polarized light digital image showing biotite in a network of weakly oriented grains along with sapphirine and garnet defining a foliation; d: Crossed polarized light digital image of partial rim of biotite along resorbed porphyroblast garnet boundaries with few small grains of sapphirine; e: and f: Crossed polarized light image of garnet porphyroblasts containing sapphirine–orthopyroxene symplectites rimmed by cordierite at its margins. Cordierite occurs as corona on sapphirine–orthopyroxene symplectites. Small euhedral garnets (shown by arrow) occur between the symplectites.

Sapphirine + quartz (Fig. 6c) along with biotite also occur outside the garnet porphyroblasts in the same sample. Sapphirine + orthopyroxene intergrowths occur around biotite (Fig. 6d).

4. Mineral chemistry

Mineral chemical data were obtained using a CAMECA SX−100 EPMA at the Indian Bureau of Mines, Nagpur, India. All the thin sections were carbon coated prior to study by Boc Edwards Auto 306 Carbon coating equipment. A beam current of 12 nA and an acceleration voltage of 15 kV were used along with a beam diameter of 1 μm. Wave-length dispersive spectrometry was employed using four vertical spectrometers. Various standards supplied by BRGM, France, were used to calibrate the instruments. The analyzed elements along with the calibrated standard and the crystal used for WDS analysis in both the instruments are as follows: Si & Na (albite on TAP crystal), Al (corundum on TAP crystal), Mg (periclase on TAP crystal), Ca (andradite on TAP crystal), K (orthoclase on PET crystal), Mn & Ti (MnTiO$_3$ on LIF crystal), Fe (Hematite on LIF crystal), P (apatite on TAP crystal), Zn (Sphalerite on LLIF crystal) and Cr (chromite on LLIF crystal). K alpha X-ray emission lines of all the above elements were used for calibration. On-line peak stripping and corrections were performed using PEAKSIGHT software supplied by CAMECA. After repeated analyses of respective standards listed above along with the minerals of interest, it was observed that the error on the elements did not exceed ±1%. A summary of the mineral chemical data is given along with mineral assemblages and melt features in Table 1. The representative compositions of minerals in the analyzed samples are given in Tables 2−8 and individual mineral compositions are discussed below. Fe^{3+} for various minerals was calculated using charge balance.
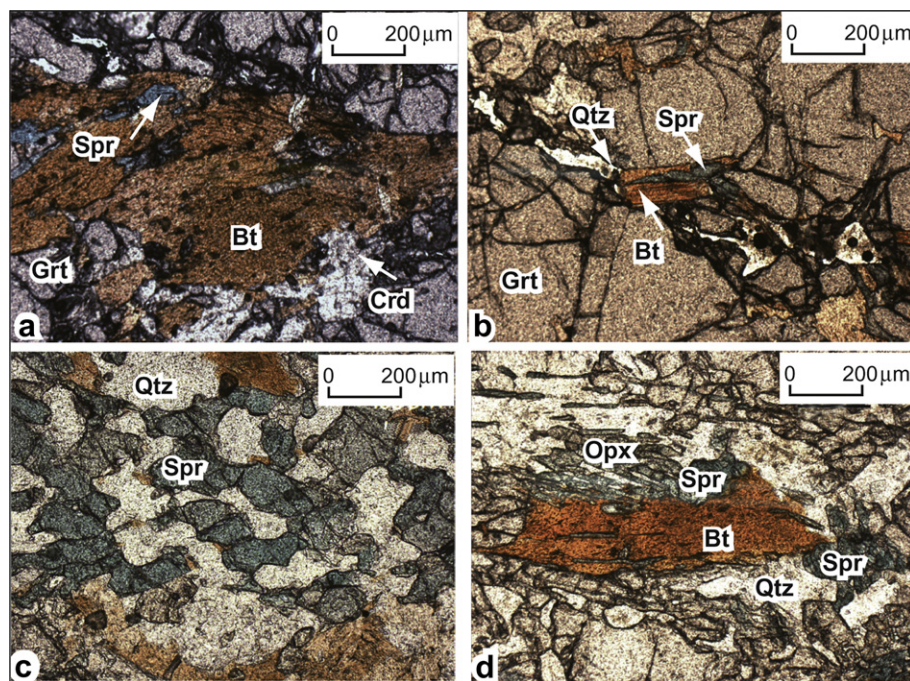
4.1. Garnet

Garnet porphyroblasts in metapelites are a pyrope-almandine solid solution (pyrope 37%−49%, almandine 44%−57%), with minor grossular (up to 4.2%), spessartine (1.21%−1.53%) and low andradite (<0.41) components (Table 2). The garnets are characterized by homogeneous core compositions with low magnesium content (x_{Mg} = 0.47) and slightly higher calcium and manganese content relative to the rims (x_{Mg} = 0.60). The garnet in migmatite is a pyrope−almandine solid solution (pyrope 38%−42%, almandine 52%−55%), with minor grossular (up to −3.5%), spessartine (1.5%−1.4%) and low andradite (<2.6%) components (Table 2). The core and rim compositions of garnets in migmatite (x_{Mg} = 0.57−0.59) do not show much variation in terms of iron, calcium and manganese contents, except that it has andradite rich rims (2.66 mol%) compared to core (0.67 mol%).

The garnet composition in the leptynite gneiss (sample P-51b) is also almandine−pyrope (almandine 52%−55%, pyrope 38%−42%) but has slightly lower x_{Mg} = 0.39−0.41 compared to the garnet in metapelitic rocks and sapphirine granulites. Cores of small idiomorphic garnets in sapphirine granulite (sample P-61a) have compositions that are less rich in Mg (pyrope 51.8 mol%, almandine 42.3%) in comparison with larger garnets with Spr and Crd which have up to pyrope 59 mol%, almandine 36 mol% (sample P-61b). The small garnet possess lower (x_{Mg} = 0.46−0.51) than that of the larger grains (x_{Mg} = 0.50−0.60).

4.2. Orthopyroxene

Orthopyroxene analyses are presented in Table 3. The orthopyroxene porphyroblasts are characterized by a systematic decrease in the Al$_2$O$_3$ content from core ($w(Al_2O_3)$ = 7.65%−9.86%) to rim ($w(Al_2O_3)$ = 6.86%−7.22%) followed by an increase in MgO

Figure 6   a: The sapphirine and biotite in a foliated microstructure within porphyroblast garnet in sample 61b; b: Sapphirine + quartz within porphyroblast garnet; c: Sapphirine + quartz along with biotite outside the garnet porphyroblasts in the same sample; d: Sapphirine + orthopyroxene intergrowths around biotite in sample 61b.

Table 2 Representative garnet analyses.

Sample	TK-12	TK-12	TK-10	TK-10	P-51B	P-51B	P-61a	P-61a	P-61b	P-61b
Location	c	r	c	r	c	r	c	r	c	r
SiO_2	39.90	39.88	39.00	38.10	38.96	39.12	39.82	39.91	40.06	39.76
TiO_2	0.10	0.12	0.10	0.10	0.06	0.09	0.10	0.12	0.08	0.04
Al_2O_3	22.80	22.27	22.10	22.50	22.06	22.47	22.23	22.91	23.68	22.54
Fe_2O_3	0.10	0.00	0.20	0.90	0.39	0.00	1.00	0.00	0.09	0.37
FeO	21.50	26.78	26.20	26.21	26.37	26.96	21.02	22.21	18.88	22.80
MnO	0.70	0.56	0.71	0.70	0.72	0.65	0.41	0.92	0.82	1.28
MgO	13.30	9.76	10.21	10.80	10.15	9.88	13.81	12.28	15.86	12.86
CaO	1.80	1.55	1.51	1.52	1.52	1.46	1.92	1.63	1.06	0.84
Total	100.20	100.92	100.03	100.83	100.23	100.63	100.31	99.98	100.53	100.49
Si	2.980	3.017	2.987	2.910	2.980	2.980	2.976	2.994	2.941	2.981
Al^{iv}	0.020	0.000	0.013	0.090	0.020	0.020	0.024	0.006	0.059	0.019
Al^{vi}	1.987	1.090	1.995	2.026	1.971	1.998	1.935	2.023	1.990	1.974
Ti	0.004	0.007	0.003	0.005	0.003	0.005	0.003	0.005	0.004	0.002
Fe^{3+}	0.008	0.000	0.000	0.000	0.023	0.000	0.055	0.000	0.005	0.021
Fe^{2+}	1.346	1.711	1.677	1.670	1.687	1.721	1.313	1.427	1.159	1.429
Mn	0.046	0.036	0.047	0.042	0.047	0.042	0.023	0.055	0.051	0.081
Mg	1.479	1.101	1.160	1.227	1.157	1.122	1.542	1.361	1.736	1.437
Ca	0.140	0.126	0.125	0.119	0.125	0.119	0.150	0.125	0.083	0.067
Total	8.010	7.986	8.007	8.052	8.012	8.007	8.021	7.996	8.028	8.012
Almandine	44.11	57.55	55.42	52.30	55.42	56.95	42.38	48.07	36.41	46.79
Andradite	0.41	0.00	0.67	2.66	1.14	0.00	2.77	0.00	0.25	1.06
Grossular	4.29	4.23	3.51	1.45	3.04	4.00	2.27	4.22	2.58	1.21
Pyrope	49.65	37.02	38.84	42.16	38.84	37.65	51.81	45.86	59.02	48.22
Spessartine	1.53	1.21	1.57	1.44	1.57	1.41	0.77	1.86	1.73	2.73
x_{Mg}	0.47	0.60	0.59	0.57	0.41	0.39	0.46	0.51	0.60	0.50

Note: the unit of the oxides is %.

content from core ($x_{Mg} = 0.68-0.78$) to rim ($x_{Mg} = 0.70-0.86$) regardless of whether the orthopyroxene occurs in garnet-free or garnetiferous sapphirine granulites (Table 3). Such variation and high aluminum content in orthopyroxene were previously reported in other granulites facies rocks from the Eastern Ghats granulite belt (e.g., Lal et al., 1987; Sengupta et al., 1990; Bhattacharya and Kar, 2002) and have also been recorded from typical UHT granulites elsewhere (e.g., Harley, 1998a, b). The high Al in the homogeneous core could reflect growth of the orthopyroxene during peak metamorphic conditions, whereas the lower Al content in the rims could reflect its growth history during the cooling stage. In terms of magnesium contents, orthopyroxene in sample P-62 with highly refractory assemblage posses the highest magnesium composition ($x_{Mg} = 0.85$) and the sillimanite absent assemblage in sample P-61b has the lowest x_{Mg} (=0.70).

4.3. Sapphirine

Sapphirine compositional plot is shown in Fig. 7. Their $w(Al_2O_3)$ content shows a range of 56.8%−64% (Table 4). The composition of coarse sapphirine in sapphirine granulites ($w(FeO) = 3.74\%-8.13\%$) is less ferran compared to that of the rare sapphirine ($w(FeO) = 8.43\%-9.12\%$) occurring as elongate inclusions in garnet along with quartz. The sapphirine rim associated with porphyroblast spinel in sample P-62 has the highest $w(Al_2O_3)$ content (63.95%) and a formula close to the ideal 7:9:3 end member (Fig. 7), assuming Fe and Mg exchange on sites. Calculated Fe^{3+} of all sapphirines is low, less than 0.27 p.f.u. The x_{Mg} varies from 0.75 to 0.90 and no clear variation between core and rim was detected.

4.4. Biotite

Biotite in the matrix of pelitic granulites and leptynite gneiss has high TiO_2 (2.43−3.89), high $x_{Mg} = 0.76-0.86$ and low Al^{vi} (<0.25) and comparatively higher TiO_2 (3.96−4.86), higher $x_{Mg} = 0.86-0.89$ and lower Al^{vi} (<0.20) than those in the sapphirine granulites (Table 5). The matrix biotite associated with sapphirine and spinel in sample P-62 has the highest x_{Mg} (=0.89). The biotite is highly magnesian, with x_{Mg} varying from 0.76 to 0.89, indicating magnesian bulk compositions of their protoliths.

4.5. Cordierite

Cordierite is mostly dry, as indicated by the high totals (above 100%) and the absence of alkalis (see Vry et al., 1990). Mineral formulas calculated on the basis of 18 oxygens indicate Si uniformly above 5 and Al consistently below 4 (Table 6) similar to the situation ($Si^+ = Al^+$) proposed by Schreyer et al. (1990). Cordierite is the most magnesian phase ($x_{Mg} = 0.87-0.92$) in these rocks.

4.6. Plagioclase

Plagioclase composition varies in quartz-rich domains in metapelitic rocks and has x_{An} varying from An_{68} to An_{51} (Table 7). The plagioclase composition in sapphirine-rich rocks is lower and shows a narrower range ($x_{An} = 0.44-0.51$). The coarse plagioclase associated with orthopyroxene in garnet-bearing sapphirine granulite sample P-62 has $x_{An} = 0.44$. Plagioclase in leptynite

Table 3 Selected orthopyroxene compositions.

Sample	P-63	P-63	P-60	P-60	P-62	P-62	P-61a	P-61a	P-61b	P-61b
	c	r	c	r	c	r	c	r	c	r
SiO_2	47.86	47.98	49.68	50.45	50.12	52.67	49.86	49.96	48.72	49.17
Al_2O_3	9.86	8.72	8.66	7.85	8.78	6.86	7.65	7.22	8.78	8.22
TiO_2	0.15	0.09	0.08	0.08	0.08	0.02	0.12	0.14	0.14	0.06
Cr_2O_3	0.01	0.02	0.00	0.00	0.00	0.00	0	0	0.05	0.02
FeO	20.26	20.48	14.76	16.32	17.34	10.85	16.37	16.45	19.28	19.48
MnO	0.34	0.38	0.08	0.08	0.08	0.08	0.18	0.16	0.18	0.12
MgO	21.76	22.52	26.56	25.68	24.05	30.24	26.12	25.76	22.76	23.12
CaO	0.08	0.07	0.06	0.06	0.06	0.06	0.08	0.05	0.04	0.02
Sum	100.32	100.26	99.88	100.52	100.51	100.78	100.38	99.74	99.95	100.21
Oxygens	6	6	6	6	6	6	6	6	6	6
Si	1.750	1.754	1.795	1.804	1.807	1.831	1.783	1.802	1.781	1.791
Al	0.425	0.376	0.368	0.331	0.372	0.281	0.322	0.307	0.378	0.353
Ti	0.004	0.002	0.002	0.002	0.002	0.000	0.003	0.004	0.004	0.002
Fe^{3+}	0.065	0.112	0.036	0.055	0.010	0.055	0.104	0.082	0.052	0.061
Fe^{2+}	0.554	0.514	0.409	0.432	0.512	0.260	0.385	0.414	0.537	0.533
Mn	0.010	0.011	0.002	0.002	0.002	0.002	0.005	0.005	0.006	0.004
Mg	1.189	1.229	1.386	1.372	1.293	1.569	1.393	1.384	1.24	1.255
Ca	0.003	0.002	0.002	0.002	0.002	0.002	0.005	0.002	0.002	0.00
Cation total	4.000	4.000	4.000	4.000	4.000	4.000	4.000	4.000	4.000	4.000
Ca	0.002	0.002	0.001	0.001	0.001	0.002	0.001	0.001	0.001	0.00
Mg	0.680	0.703	0.77	0.759	0.716	0.715	0.782	0.769	0.697	0.702
Fe	0.318	0.295	0.229	0.24	0.283	0.283	0.217	0.23	0.302	0.298
x_{Mg}	0.68	0.71	0.77	0.76	0.72	0.86	0.78	0.77	0.70	0.70

Note: the unit of the oxides is %.

Table 4 Selected sapphirine compositions.

Sample	P-63	P-63	P-60	P-60	P-62	P-62	P-61a	P-61b
Location	c	c	c	r	c	r	c	c
SiO_2	13.77	13.56	12.68	13.67	14.42	11.12	16.28	14.99
TiO_2	0.06	0.02	0.00	0.08	0.02	0.06	0.07	0.11
Al_2O_3	61.12	60.78	62.46	61.42	60.54	63.95	56.78	58.74
Cr_2O_3	0.00	0.00	0.00	0.00	0.00	0.00	0.03	0.02
Fe_2O_3	0.00	2.55	2.77	1.05	1.56	3.06	0.00	0.00
FeO	7.98	4.37	6.89	8.13	3.74	5.21	8.43	9.12
MnO	0.08	0.09	0.09	0.06	0.09	0.12	0.02	0.04
MgO	15.88	17.85	15.88	15.86	18.86	15.67	16.93	15.62
CaO	0.00	0.00	0.00	0.00	0.00	0.00	0.26	0.14
Total	98.91	98.99	100.51	100.18	99.09	98.90	98.80	98.78
Oxygens	20	20	20	20	20	20	20	20
Si	1.658	1.616	1.506	1.63	1.707	1.334	1.965	1.815
Ti	0.005	0.002	0.000	0.007	0.002	0.005	0.006	0.01
Al	8.675	8.539	8.744	8.634	8.447	9.047	8.08	8.387
Cr	0.000	0.000	0.000	0.000	0.000	0.000	0.003	0.002
Fe^{3+}	0.000	0.226	0.245	0.092	0.136	0.274	0.000	0.000
Fe^{2+}	0.803	0.439	0.686	0.813	0.373	0.525	0.851	0.924
Mn	0.008	0.009	0.009	0.006	0.009	0.012	0.002	0.004
Mg	2.849	3.17	2.81	2.818	3.327	2.802	3.046	2.819
Ca	0.000	0.000	0.000	0.000	0.000	0.000	0.034	0.018
Sum	14.000	14.000	14.000	14.000	14.000	14.000	13.987	13.98
x_{Mg}	0.78	0.88	0.80	0.78	0.90	0.84	0.78	0.75

Note: the unit of the oxides is %.

Table 5   Selected biotite compositions.

Sample	TK-12	TK-12	TK-10	TK-10	P-51B	P-60	P-60	P-62	P-62	P-61a	P-61b
Location	c	r	c	r	c	c	r	c	r	c	c
SiO_2	37.68	39.81	41.00	39.73	39.33	41.24	39.85	41.38	41.56	39.82	41.56
TiO_2	3.89	3.12	3.12	2.43	3.58	3.96	4.64	4.62	4.38	4.16	4.86
Al_2O_3	13.96	13.98	11.28	13.45	12.77	12.88	13.33	13.38	13.56	15.34	13.65
FeO	10.32	7.8	6.41	6.91	8.76	6.54	5.82	4.78	4.82	5.10	4.98
MnO	0.03	0.00	0.00	0.01	0.00	0.03	0.03	0.04	0.04	0.05	0.03
MgO	19.05	21.49	22.17	19.82	21.38	23.96	20.87	22.32	21.96	24.16	21.85
CaO	0.00	0.14	0.47	0.12	0.04	0.05	1.00	0.02	0.03	0.05	0.05
Na_2O	0.18	0.28	0.22	0.13	0.07	0.21	0.16	0.42	0.37	0.12	0.21
K_2O	10.11	9.42	7.98	8.85	10.51	9.84	9.56	10.12	10.21	9.88	10.28
Total	95.22	96.04	92.65	91.45	96.44	98.71	95.26	97.08	96.93	98.68	97.47
Oxygens	22	22	22	22	22	22	22	22	22	22	22
Si	5.542	5.686	5.979	5.901	5.669	5.708	5.709	5.778	5.809	5.482	5.782
Ti	0.43	0.335	0.342	0.271	0.388	0.412	0.5	0.485	0.46	0.431	0.508
Al^{iv}	2.42	2.314	1.939	2.099	2.171	2.101	2.251	2.202	2.191	2.489	2.218
Al^{vi}	0.000	0.040	0.000	0.255	0.000	0.000	0.000	0.000	0.004	0.000	0.020
Fe	1.27	0.932	0.782	0.858	1.056	0.757	0.697	0.558	0.563	0.587	0.579
Mn	0.004	0.000	0.000	0.001	0	0.004	0.004	0.005	0.005	0.006	0.004
Mg	4.177	4.576	4.82	4.388	4.594	4.943	4.457	4.646	4.576	4.958	4.531
Ca	0.000	0.021	0.073	0.019	0.006	0.007	0.153	0.003	0.004	0.007	0.007
Na	0.051	0.078	0.062	0.037	0.02	0.056	0.044	0.114	0.1	0.032	0.057
K	1.897	1.716	1.484	1.677	1.93	1.737	1.747	1.802	1.820	1.735	1.824
OH	4.000	4.000	3.110	3.055	4.000	4.000	4.000	4.000	4.000	4.000	4.000
Total	19.791	19.698	18.591	18.561	19.833	19.725	19.562	19.594	19.573	19.727	19.53
x_{Mg}	0.77	0.83	0.86	0.84	0.81	0.87	0.87	0.89	0.89	0.89	0.89

Note: the unit of the oxides is %.

sample P-51b has distinctly higher x_{An} content of 0.69 and coarse plagioclase associated with spinel in sapphirine granulite sample P-62 has the lowest x_{An} (0.44) observed in this study. The *alkali feldspar* is commonly orthoclase with x_{Ab} 0.27−0.41 (Table 7).

4.7. Spinel

Spinel is primarily spinel-hercynite solid solution with very little magnetite and gahnite contents (Table 8). x_{Mg} varies from 0.34 to 0.59 and is less magnesian than the coexisting sapphirine

Table 6   Selected cordierite analyses.

Sample	P-63	P-60	P-62	P-61a
SiO_2	51.14	50.96	51.67	52.16
Al_2O_3	33.67	33.88	33.12	33.42
FeO	2.68	3.25	2.88	1.86
MnO	0.09	0.05	0.05	0.05
MgO	12.96	12.46	12.56	12.64
Sum	100.54	100.6	100.28	100.13
Si	5.018	5.008	5.08	5.107
Al	3.895	3.925	3.839	3.857
Fe	0.22	0.267	0.237	0.152
Mn	0.007	0.004	0.004	0.004
Mg	1.895	1.825	1.84	1.844
x_{Mg}	0.9	0.87	0.89	0.92

Note: the unit of the oxides is %.

(0.77−0.89) and biotite (0.76−0.89). TiO_2 content is low (<0.006). Zn content is negligible (<0.003) and hence not shown.

5. Micro-structural relations and reactions

Sapphirine-bearing UHT granulites commonly preserve mineral reaction microstructures such as coronas and intergrowths that record evidence of overstepped mineral reactions that crossed during the $p−T$ evolution. The development and preservation of these microstructures depend on reaction kinetics, diffusion rates and the presence of an appropriate grain boundary medium to enhance diffusion. Although evidence of the prograde evolution is commonly overprinted by the metamorphic peak mineral assemblage, microstructures such as these may preserve information about several portions of the retrograde segment of the $p−T$ path. The rocks of the present study include examples where the near-peak UHT mineral assemblages are preserved, but prograde history remains elusive. In others, the near-peak UHT mineral assemblages are largely overprinted by reaction during the retrograde evolution. The granulites of this study contain a near-peak assemblage of sapphirine−garnet−orthopyroxene− sillimanite−quartz−K-feldspar, which was later overprinted by intergrowth, and coronas involving sapphirine, cordierite and spinel. Biotite-rims on garnet are considered to be late assemblages. As these rocks confirm the former presence of melt, this difference in degree of retrograde reaction is attributed to the variable retention of residual melt in these rocks after the peak of metamorphism.

The leucocratic layers in the metapelitic granulite and leuco-some in migmatites can be considered to represent at least a part

Table 7 Selected feldspar compositions.

Sample	TK-12	TK-12	TK-10	P-62	P-60	P-60	P-51B	TK-12	TK-12	P-60	P-51B
	Pl	Pl	Pl	Pl	Pl	Pl	Pl	Kfs	Kfs	Kfs	Kfs
	Core	Discrete	Core	Core	Core	Rim	Rim	Core	Rim	Core	Core
	Qtz rich domains		Discrete								
SiO_2	56.24	56.17	62.58	59.81	57.72	57.54	56.12	65.81	66.21	66.23	66.12
TiO_2	0.00	0.00	0.00	0.09	0.02	0.04	0.00	0.00	0.00	0.00	0.00
Al_2O_3	28.26	27.68	25.48	25.73	26.88	27.12	28.37	19.67	19.46	18.28	18.77
FeO	0.4	0.31	0.00	0.13	0.22	0.18	0.16	0.00	0.00	0.00	0.00
MnO	0.01	0.02	0.1	0.00	0.04	0.02	0.00	0.00	0.00	0.00	0.00
MgO	0.03	0.06	0.15	0.53	0.05	0.04	0.06	0.00	0.00	0.00	0.00
CaO	10.23	10.14	5.84	5.58	10.12	9.98	10.65	1.38	1.14	0.28	1.21
Na_2O	5.74	5.62	5.68	6.93	5.28	5.55	5.56	4.74	4.32	3.12	4.77
K_2O	0.00	0.00	0.00	0.00	0.00	0.00	0.00	9.26	9.97	12.86	9.64
Total	100.91	100	99.83	98.8	100.33	100.47	100.92	100.86	101.1	100.77	100.51
Oxygens	8	8	8	8			8	8	8	8	8.00
Si	2.507	2.524	2.746	2.675	2.576	2.566	2.501	2.951	2.966	3.005	2.980
Ti	0.000	0.000	0.000	0.003	0.001	0.001	0.000	0.00	0.00	0.00	0.000
Al	1.485	1.466	1.318	1.357	1.414	1.426	1.491	1.04	1.028	0.978	0.997
Fe	0.013	0.011	0.000	0.004	0.008	0.01	0.005	0.00	0.00	0.00	0.000
Mn	0.000	0.001	0.004	0.000	0.002	0.001	0.000	0.00	0.00	0.00	0.000
Mg	0.002	0.004	0.010	0.035	0.003	0.003	0.004	0.00	0.00	0.00	0.000
Ca	0.489	0.488	0.275	0.267	0.484	0.477	0.509	0.066	0.055	0.014	0.058
Na	0.496	0.49	0.483	0.601	0.457	0.48	0.481	0.412	0.375	0.274	0.417
K	0.000	0.000	0.000	0.000	0.000	0.000	0.000	0.53	0.57	0.744	0.554
Sum	4.992	4.984	4.836	4.942	4.945	4.960	4.991	4.999	4.994	5.015	5.007
x_{an}	0.68	0.68	0.51	0.44	0.51	0.5	0.69	0.12	0.14	0.26	0.540

Note: the unit of the oxides is %.

Table 8 Selected spinel compositions.

Sample	P-60	P-60	P-62	P-62
Location	c	r	c	r
SiO_2	0.01	0.03	0.01	0.02
TiO_2	0.28	0.05	0.02	0.00
Al_2O_3	60.57	56.88	58.98	59.07
Cr_2O_3	0.78	0.06	0.28	0.25
Fe_2O_3	0.73	9.25	7.83	7.11
FeO	28.61	18.8	19.6	18.38
MnO	0.11	0.06	0.07	0.06
MgO	8.52	14.34	14.36	14.89
Total	99.54	98.55	100.38	99.07
Oxygens	4.000	4.000	4.000	4.000
Si	0.00	0.001	0.00	0.001
Ti	0.006	0.001	0.00	0.00
Al	1.956	1.808	1.837	1.852
Cr	0.017	0.001	0.006	0.005
Fe^{3+}	0.015	0.187	0.155	0.142
Fe^{2+}	0.656	0.424	0.434	0.409
Mn	0.003	0.001	0.002	0.001
Mg	0.348	0.576	0.566	0.59
Sum	3.000	3.000	3.000	3.000
x_{Mg}	0.347	0.576	0.566	0.591

Note: the unit of the oxides is %.

of the melt, with some peritectic (Grt) phases (see for e.g., Moraes et al., 2002). The main melt-producing reaction in the metapelitic granulite is represented by the large amounts of sillimanite in the selvage domains (Fig. 3a and b) of metapelitic granulites:

$$Ms + Pl = Kfs + Sill + melt \tag{1}$$

The melt in this reaction is represented by leucocratic layers of quartz and K-feldspar (Fig. 3c and d). A continuous reaction responsible for garnet growth (porphyroblasts garnet, Fig. 3e) would be encountered with further heating and may be represented by the reaction:

$$Bt + Sill = Grt + Kfs + melt \tag{2}$$

The occurrence of biotite and sillimanite rimming garnet (Fig. 3f) indicates dissolution of garnet by a reaction such as:

$$Grt + Kfs \pm Crd + melt = Bt + Sill \pm Qtz \tag{3}$$

The presence of garnet−quartz and biotite−quartz intergrowths (Fig. 3d) in metapelitic migmatite is a typical feature of a retrograde reaction involving melt (see Brown, 2002). Quartz occurs only in minor amounts as inclusions in garnet (Fig. 3e) or in small pockets in the matrix associated with plagioclase ($An_{54−51}$) and near the biotite selvage (Fig. 3c) and is inferred to record the former presence of melt. It is inferred that quartz was almost completely consumed before the metamorphic peak was
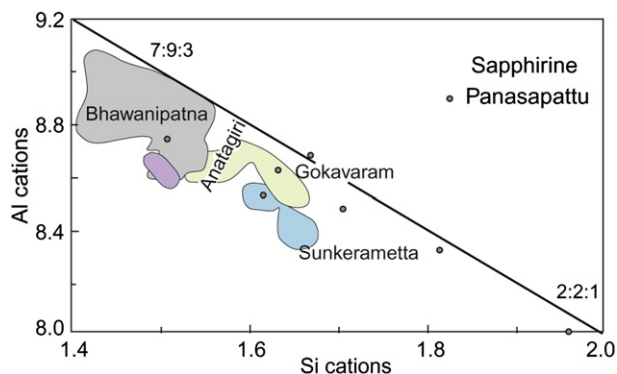
Figure 7　Compositional plot of sapphirine in Si vs. total Al. The shaded areas are the plotted fields for sapphirine reported in other areas of Eastern Ghats belt (Sengupta et al., 1990; Dasgupta et al., 1995; Bose et al., 2000).

achieved. This is consistent with melting reactions consuming quartz and suggests loss of melt.

Sheets of biotite extensively replace garnet porphyroblasts (e.g., Fig. 3f). Such replacement texture results when garnet interacts with melt as suggested by Vielzeuf and Montel (1994) by a model melting reaction such as:

$$Grt + melt = Bt + Qtz \pm Pl \tag{4}$$
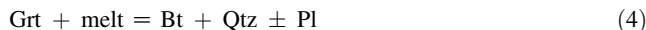
Sillimanite grains within garnet along with biotite replacing garnet porphyroblasts in leptynite gneiss may indicate garnet dissolution reaction such as reaction (3). The reaction (3) has been experimentally studied by many workers (Vielzeuf and Montel, 1994; Nair and Chacko, 2002).

The sapphirine granulite sample P-62 contains the assemblage of sapphirine and spinel in the melanocratic portion (Fig. 4e). The

absence of orthopyroxene, cordierite and quartz in these domains suggest the possible reaction:

$$Grt + Bt + Sill + Kfs = Spr + Spl + melt \tag{5}$$
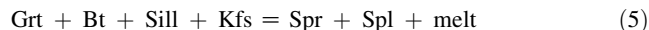
In quartz-poor sapphirine–biotite granulite (samples P-62 and P-61B), the granular-spinel-biotite within orthopyroxene–sapphirine intergrowths (Figs. 4a, 6c) may have been formed via the discontinuous KFMASH reaction:

$$Opx + Spr \pm Kfs + melt = Crd + Spl + Bt \tag{6}$$

The garnet porphyroblasts associated with sapphirine–orthopyroxene symplectites (Fig. 6c) represent the main symplecite forming reactions in the studied rocks (Fig. 4d) which produced the symplectites textures surrounding garnet.

Garnet breakdown in the absence of quartz and sillimanite produced orthopyroxene–sapphirine–cordierite symplectite at its grain boundaries (Fig. 4d). Additional formation of biotite at the expense of orthopyroxene–sapphirine symplectites by overgrowth of aggregates of biotite–cordierite can be explained through the reaction:

$$Opx + Spr + Kfs + melt = Bt + Crd + Pl \tag{7}$$

Along with the reactions (6) and (7), a new generation of small idiomorphic garnet (Grt in Fig. 5e and f) is inferred to record reaction with melt according to the FMAS (dis)continuous KFMASH reaction:

$$Opx + Crd + melt = Bt + Grt + Qtz \tag{8}$$

6. Metamorphic p–T conditions

Estimation of p–T conditions from sapphirine-bearing assemblages has been limited due to lack of suitable well-calibrated

Table 9　p–T calculated using conventional geothermobarometers.

Geothermometers T (°C)				Geobarometers p (kbar)		
	TK-12	**P-62**	**P-61a**	**Grt–Opx–Pl–Qtz**	**TK-12**	**P-62**
Haley (1984a)	816	1033	830	Perkins and Newton (1981)	7.2	12.2
Grt–Opx				Perkins and Chipera (1985)	5.2	9.57
Kawasaki and Matsui (1983)	580	765	591	Moecher et al. (1988)	6.2	6.4
Aranovich (1984)	600	782	602	Eckert et al. (1991)	7.5	12.7
Sen and Bhattacharya (1984)	703	1001	708	**Al–Opx–Grt**		
Harley (1985)	670	872	681	Harley (1984b)	6.1	9.4
Lee and Ganguly (1988)	746	989	759	**Grt–Opx**		
Bhattacharya et al. (1991)	725	915	730	Nickel and Green (1985)	12.4	10.3
Lal (1993)	605	796	619	Brey and Kohler (1990)	13.9	11.85
Pattison et al. (2003)	948	963		Pattison et al. (2003)	10.4	11
THERMOCAL v.3.1	900	915		THERMOCAL v.3.1	9.6	10.6
Pl–Kfs	**TK-12**	**TK-10**	**P-60**			
Powell and Powell (1977)	1077	657	1136			
Perchuk et al. (1985)	1578	724	1153			
Stormer and Whitney (1985)	1602	722	1612			
Stormer (1975)	1159	672	1217			
Average of previous two	1380	697	1417			
Spr–Spl	**P-62**	**P-60**				
Owen et al. (1991)	993	785				
Das et al. (2006)	965	730				
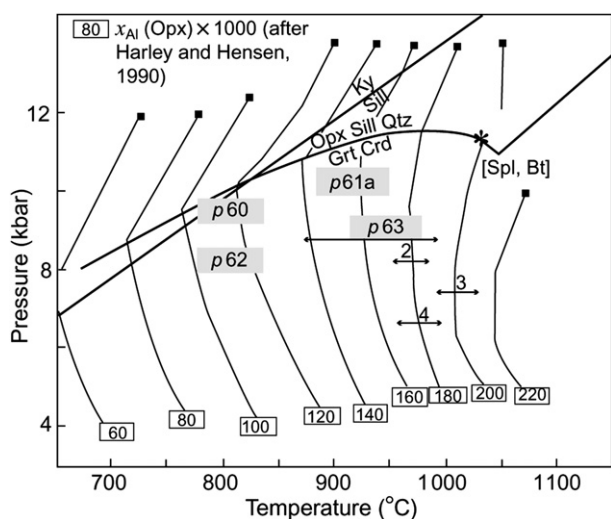
Figure 8   Selected univariant reactions in the FMAS system and isopleths of $w(Al_2O_3)$ (%) in orthopyroxene (after Harley and Motoyoshi, 2000). Calculated P and T for the UHT granulite for core to rim are shown for Opx from different grains.

thermobarometers and reliable thermodynamic data FMAS sapphirine. In practice, the full assessment of UHT p–T records should involve the analysis of rock-specific equilibrium assemblage diagrams complemented by differential isopleth diagrams, conventional thermobarometry, and semi-quantitative or qualitative theoretical analysis and evaluation of reaction textures (Harley, 2008). Therefore, metamorphic conditions have been quantified using both conventional thermobarometry and calculated isochemical sections. Calculated and contoured rock-specific equilibrium assemblage diagrams are increasingly being used for quantification of metamorphic UHT conditions of metapelitic rocks (e.g., Saha et al., 2008; Nasipuri et al., 2009). However, the conventional thermobarometers are still of value and are used in concert with the isochemical sections to ensure optimum use of all available information. This is clearly the case where the isochemical section modeling is reliant on mineral thermodynamic data that have a limited experimental basis (e.g., Fe–Mg sapphirine and oxidized systems).

6.1. Geothermobarometry

The core compositions of garnet–orthopyroxene pairs were chosen for thermo-barometric calculations. The metamorphic conditions estimated from orthopyroxene and porphyroblast garnet pairs in sapphirine granulite sample P-61a from various

geothermometrs are listed in Table 9. The results yield an average temperature of 1030 °C using the techniques of Harley (1985). The latter calibration, although more refined in a thermodynamic sense, is influenced by the feedback effects of Fe–Mg exchange on cooling (Harley, 1989; Fitzsimons and Harley, 1994; Pattison and Begin, 1994; Pattison et al., 2003) and as a consequence generally yields lower temperatures but are well within the errors associated with most thermometers in the range of ±80–100 °C. The results based on the techniques of Kawasaki and Matsui (1983), Sen and Bhattacharya (1984), Lee and Ganguly (1988), Lavrent'eva and Perchuk (1990), Bhattacharya et al. (1991) and Lal (1993) yield temperatures exceeding 1000 °C (Table 9).

The regression method of Pattison et al. (2003) was used to retrieve close to peak mineral compositions. The extent of increase in corrected temperatures is commonly up to c. 150 °C by this methodology (see Lal, 2003). The calculated p–T conditions are listed in Table 9.

A thermometer based on Fe^{2+}–Mg distribution between sapphirine and spinel provides a temperature estimate for near-peak metamorphic conditions. Owen et al. (1991) provided an empirical calibration of the Fe–Mg exchange between 2:2.1 sapphirine and spinel. As sapphirine and spinel observed in this study are within the compositional ranges of this regression, the spinel–sapphirine thermometer was applied. The results yielded a temperature of 993 °C and 965 °C for sapphirine granulite samples P-62 and P-60, respectively. These values are likely to indicate the near-peak metamorphic conditions. If we consider the effect of Fe^{3+} in sapphirine, the above estimate would be enhanced by about 40 °C indicating that the Panasapattu rocks were subjected to ultrahigh-temperature conditions. Das et al. (2011) formulated a new sapphirine–spinel geothermometer using their experimental data at 9–12 kbar and 850–1100 °C. Application of this method for stable sapphirine–spinel occurrence in sapphirine granulites (Samples P-62 and P-60) yielded almost consistent results at 940 °C and 965 °C that further confirm UHT conditions. The mineral pair sapphirine–quartz occurs in mutual contact in samples P-60, P-62 which requires a minimum T of 1030 °C–1050 °C at 10 kbar based on the FMAS model system. Aluminum content in orthopyroxene in the FMAS divariant assemblages Opx + Sill + Grt + Qtz, Opx + Grt + Spr + Qtz and Opx + Crd + 487 Grt + Qtz can be used to estimate temperatures in the samples with quartz, using Al_2O_3 isopleths in p–T space as calculated using internally consistent datasets and from combinations of experimental data and interpolation (Aranovich and Berman, 1996; Harley, 1998b; Harley and Motoyoshi, 2000). The estimated temperatures based on isopleths for the Al_2O_3 content in orthopyroxene in the FMAS assemblage Opx + Grt + Spr + Qtz (from Harley and Motoyoshi, 2000) are shown in Fig. 8. Maximum $w(Al_2O_3)$ in the analyzed

Table 10   Solution notation, formulas and model sources used for isochemical sections.

Symbol	Solution	Formula	Source
Bio(HP)	Biotite	$K[Mg_xFe_yMn_{1-x-y}]_{3-w}Al_{1+2w}Si_{3-w}O_{10}(OH)_2, {}_{x+y\leq1}$	Powell and Holland (1999)
Gt(HP)	Garnet	$Fe_{3x}Ca_{3y}Mg_{3z}Mn_{3(1-x-y-z)}Al_2Si_3O_{12}, {}_{x+y+z\leq1}$	Holland and Powell (1998)
hCrd	Cordierite	$Mg_2Fe_{2y}Mn_{2(1-x-y)}Al_4Si_5O_{18}(H_2O)_z, {}_{x+y\leq1}$	
Kf	Alkali feldspar	$Na_xK_{1-x}AlSi_3O_8$	Thompson and Hovis (1979)
melt(HP)	Melt	Na–Mg–Al–Si–K–Ca–Fe hydrous silicate melt	Holland and Powell (2001)
Sp(HP)	Spinel	$Mg_xFe_{1-x}Al_2O_3$	Ideal
Spr	Sapphirine	$Mg_{3.5}Al_9Si_{1.5}O_{20}$	Ideal
Opx(HP)	Orthopyroxene	$[Mg_xFe_{1-x}]_{2-y}Al_{2y}Si_{2-y}O_6$	Holland and Powell (1996)
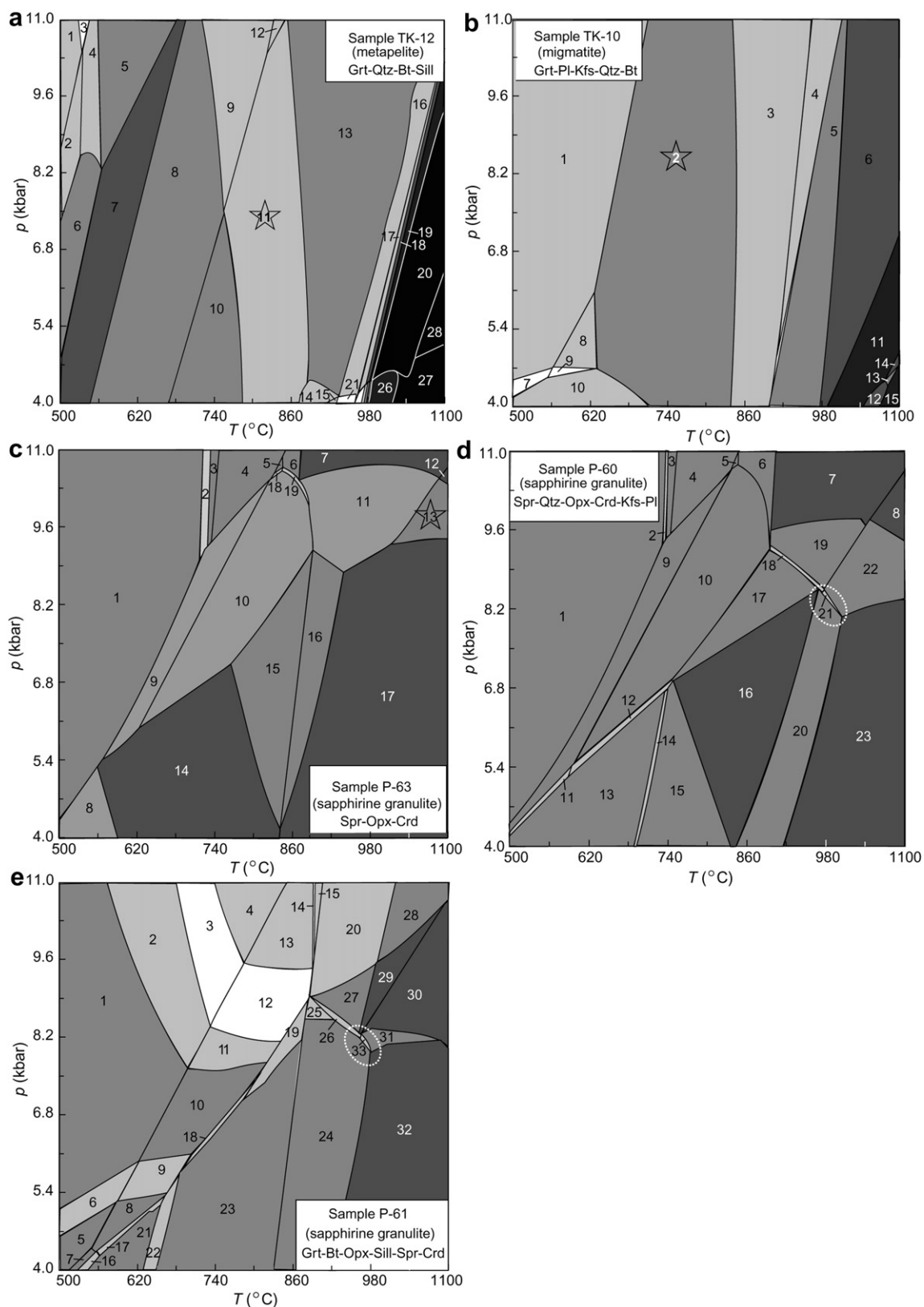
Figure 9 a: NCKFMASH *p*−*T* isochemical section for bulk composition of metapelite sample TK-12 showing the stability of Grt−Kfs−Qtz−Bt−melt. Univariant fields shown by heavy solid lines, invariant fields by light gray fill, and higher variance fields by progressively darker shading; in all isochemical sections the lowest variance fields are trivariant. 1: Bio(HP) Kf zo mu pa q; 2: Bio(HP) Pl(h) zo mu pa q; 3: Kf Bio(HP) Gt(HP) zo mu pa q; 4: Bio(HP) Pl(h) Gt(HP) mu pa q; 5: Bio(HP) Pl(h) Gt(HP) mu q; 6: Bio(HP) Pl(h) mu pa q; 7: Bio(HP) Pl(h) mu q; 8: Bio(HP) Pl(h) mu san q; 9: Bio(HP) Pl(h) Gt(HP) mu san q; 10: Bio(HP) Pl(h) sill san q; 11: Bio(HP) Pl(h) Gt(HP) sill san q; 12: Bio(HP) Pl(h) Gt(HP) ky san q; 13:

orthopyroxene is 9.86%, which implies a maximum temperature around 1080 °C.

For the assemblage garnet−orthopyroxene−plagioclase−quartz in the sapphirine granulite P-62, the formulation of Pattison et al. (2003) was employed, using a convergence technique and accounts for the late Fe−Mg exchange. For comparison, results obtained for this sample from the THERMOCALC program (ver. 3.1) (Holland and Powell, 1998) are also given. The pressures calculated by Nickel and Green (1985) and other geobarometers yielded much higher pressures of up to 13.9 kbar (Table 9).

6.2. Isochemical section modeling

The p−T conditions for these samples have also been investigated using isochemical modeling. Most calculations of melting processes in metapelitic compositions can be adequately expressed in the model system $Na_2O-CaO-K_2O-FeO-MgO-Al_2O_3-SiO_2-H_2O-TiO_2-Fe_2O_3$ (NCKFMASH) (White et al., 2001; White and Powell, 2002). The NCKFMASH p−T isochemical sections for the p−T range 600−1000 °C and 4−11 kbar were computed using the PERPLEX software (Connolly, 2005; for the bulk compositions of the samples see Table 9). The following phases and the corresponding phase components were used (abbreviations in the program), Spr7 [spr7, fspr], Crd [crd, fcrd, hcrd, hfcrd], Crn, Spl [spl, herc], Opx [en, fs, mgts], Bt [ann, phl, east], Kfs, Sill, Qtz, and silicate melt phase [h2OL, fo8L, fa8L, sil8L, kspL]. K-feldspar, sillimanite and quartz were taken to be pure phases. The solution models (details in solut09.dat; PERPLEX 07; database: hp04ver.dat) adopted are Opx (HP), Sp (HP), Sapp (HP), Bio (HP), hCrd and Melt (HP). Table 10 indicates the general formula and references for each solution model used. For hydrous fluids, the solution model of Kerrick and Jacobs (1981) was adopted. The subsequent solid-solution models (e.g., Powell and Holland, 1999), being compatible with this data set, were selected from the downloaded version of the PERPLEX solution-model file (solut09.dat). The obtained graphical results (subprograms VERTEX and PSVDRAW) were taken as raw data, and the final diagrams were redrawn by smoothing curves as demonstrated by Connolly (2005). Divariant phase fields are unfilled; tri and quadrivariant phase fields are in increasing shades of gray. A series of p−T isochemical sections relevant to the melt-bearing mineral assemblages preserved in these rocks are presented in Fig. 9a−e, the observed minerals and mineral assemblages of the various samples in this study appear in the isochemical section for their bulk composition in the considered p−T range.

A critical consideration in the calculation of these isochemical sections is the estimation of an appropriate bulk chemical composition, which must take into account the equilibration volume of the mineral assemblage observed in thin section. For medium- to high-grade rocks, a representative bulk composition is commonly estimated using molecular proportions recalculated from X-ray fluorescence (XRF) analyses (e.g., Kelsey et al., 2005). This method has been applied in the present study and is presented in Table 11. The H_2O content in the system was reduced approximately to the point that the assemblage was just saturated

Pl(h) Gt(HP) sill san q; 14: Pl(h) Gt(HP) sill hcrd san q; 15: Pl(h) Gt(HP) sill crd san q; 16: Pl(h) Kf Gt(HP) sill san q; 17: melt(HP) Pl(h) Gt(HP) sill san q; 18: melt(HP) Gt(HP) sill san; 19: melt(HP) Gt(HP) sill; 20: melt(HP) Gt(HP); 21: Pl(h) Kf Gt(HP) sill crd san q; 22: melt(HP) Pl(h) Gt(HP) sill crd san q; 23: melt(HP) Pl(h) Gt(HP) sill crd san; 24: melt(HP) Pl(h) Gt(HP) crd san; 25: melt(HP) Pl(h) Gt(HP) crd; 26: melt(HP) Gt(HP) crd; 27: melt(HP) crd; 28: melt(HP) hcrd.

b: NCFMASH p−T isochemical section for migmatite sample TK-10 showing the stability of Grt−Pl−Kfs−Qtz−Bt−melt. 1: Bio(HP) Gt(HP) ky san q; 2: Bio(HP) Gt(HP) san q; 3: Bio(HP) melt(HP) Gt(HP) san q; 4: melt(HP) Gt(HP) en san q; 5: melt(HP) Gt(HP) en q; 6: melt(HP) Gt(HP) q; 7: Bio(HP) Gt(HP) osm1 ky san q; 8: Bio(HP) Gt(HP) sill san q; 9: Bio(HP) Gt(HP) osm1 sill san q; 10: Bio(HP) Gt(HP) osm1 san q; 11: melt(HP) Gt(HP); 12: melt(HP) Gt(HP) crd; 13: melt(HP) Gt(HP) crd en; 14: melt(HP) Gt(HP) en; 15: melt(HP) crd.

c: NCFMASH p−T isochemical section for bulk composition of sapphirine granulite sample P-63 showing the stability of Spr−Opx−Crd−melt assemblage; 1: Bio(HP) Opx(HP) ky ta; 2: Bio(HP) Opx(HP) ky sud ta; 3: Bio(HP) Opx(HP) ky sud; 4: Bio(HP) Opx(HP) ky H_2O; 5: Bio(HP) Opx(HP) sill H_2O; 6: Bio(HP) melt(HP) Opx(HP) sill; 7: melt(HP) Opx(HP) sill; 8: Bio(HP) hCrd Opx(HP) ta; 9: Bio(HP) hCrd Opx(HP) ky; 10: Bio(HP) hCrd Opx(HP) sill; 11: melt(HP) hCrd Opx(HP) sill; 12: melt(HP) Sapp(HP) Opx(HP); 13: melt(HP) Sapp(HP) hCrd Opx(HP); 14: Bio(HP) hCrd Opx(HP); 15: Bio(HP) hCrd Opx(HP) san; 16: melt(HP) hCrd Opx(HP) san; 17: melt(HP) hCrd Opx(HP); 18: Bio(HP) hCrd Opx(HP) sill H_2O; 19: Bio(HP) melt(HP) hCrd Opx(HP) sill.

d: NCFMASH p−T isochemical section for bulk composition of sapphirine granulite sample P-60 showing the stability of Spr−Opx−Kfs−Sill assemblage; 1: Bio(HP) Opx(HP) ky ta; 2: Bio(HP) Opx(HP) ky sud ta; 3: Bio(HP) Opx(HP) ky sud; 4: Bio(HP) Opx(HP) ky H_2O; 5: Bio(HP) Opx(HP) sill H_2O; 6: Bio(HP) melt(HP) Opx(HP) sill; 7: melt(HP) Opx(HP) sill; 8: melt(HP) Sapp(HP) Opx(HP); 9: Bio(HP) hCrd Opx(HP) ky; 10: Bio(HP) hCrd Opx(HP) sill; 11: Bio(HP) hCrd Opx(HP) osm1 ky; 12: Bio(HP) hCrd Opx(HP) osm1 sill; 13: Bio(HP) hCrd Opx(HP) osm1; 14: Bio(HP) hCrd Opx(HP) osm1 san; 15: Bio(HP) hCrd Opx(HP) san; 16: hCrd Opx(HP) san; 17: hCrd Opx(HP) sill san; 18: melt(HP) hCrd Opx(HP) sill san; 19: melt(HP) hCrd Opx(HP) sill; 20: melt(HP) hCrd Opx(HP) san; 21: melt(HP) Sapp(HP) hCrd Opx(HP) san; 22: melt(HP) Sapp(HP) hCrd Opx(HP); 23: melt(HP) hCrd Opx(HP).

e: NCFMASH p−T isochemical section for bulk composition of sapphirine granulite sample P-61 showing the stability of Bt−Spr−Opx−Crd−Pl−Kfs−melt assemblage. 1: Bio(HP) Opx(HP) ky san; 2: Bio(HP) Gt(HP) Opx(HP) ky san; 3: Bio(HP) Gt(HP) Opx(HP) ky san q; 4: Bio(HP) Gt(HP) ky san q; 5: Bio(HP) Opx(HP) osm1 ky; 6: Bio(HP) Opx(HP) osm1 ky san; 7: Bio(HP) Opx(HP) osm1; 8: Bio(HP) Opx(HP) osm1 sill; 9: Bio(HP) Opx(HP) osm1 sill san; 10: Bio(HP) Opx(HP) sill san; 11: Bio(HP) Gt(HP) Opx(HP) sill san; 12: Bio(HP) Gt(HP) Opx(HP) sill san q; 13: Bio(HP) Gt(HP) sill san q; 14: Bio(HP) melt(HP) Gt(HP) sill san q; 15: Bio(HP) melt(HP) Gt(HP) sill san; 16: Bio(HP) hCrd Opx(HP) osm1; 17: Bio(HP) hCrd Opx(HP) osm1 sill; 18: Bio(HP) hCrd Opx(HP) sill san; 19: Bio(HP) hCrd Gt(HP) Opx(HP) san; 20: melt(HP) Gt(HP) Opx(HP) sill san; 21: Bio(HP) hCrd Opx(HP) osm1; 22: Bio(HP) hCrd Opx(HP) osm1 san; 23: Bio(HP) hCrd Opx(HP) san; 24: melt(HP) hCrd Opx(HP) san; 25: melt(HP) hCrd Gt(HP) Opx(HP) san; 26: melt(HP) hCrd Opx(HP) sill san; 27: melt(HP) Opx(HP) sill san; 28: melt(HP) Gt(HP) Opx(HP) sill; 29: melt(HP) Opx(HP) sill; 30: melt(HP) Sapp(HP) Opx(HP); 31: melt(HP) Sapp(HP) hCrd Opx(HP); 32: melt(HP) hCrd Opx(HP); 33: melt(HP) Sapp(HP) hCrd Opx(HP) san.

immediately subsolidus at 6 kbar, following the procedure reported by White et al. (2001). The paucity of oxide minerals in the studied samples suggests that Fe^{3+} in the bulk compositions is low. Fe^{3+} was estimated by recalculating mineral analysis to incorporate Fe^{3+}. Since O rather than Fe^{3+} is the natural variable Fe_2O_3 has been recast as "O" in the bulk compositions. Magnetite, ilmenite, rutile and lower-T (~500 °C–600 °C) part of the pseudosections occurring as phases stable in this range such as chloritoid, chlorite, ortho-amphibole and staurolite have not been shown in the presented isochemical sections for clarity.

Two Si-saturated metapelites and three high Mg–Al granulites were chosen for the calculation of p–T isochemical sections. They share the same metamorphic histories and have experienced similar peak p–T conditions (i.e., local field gradients, if present, were insignificant). The bulk compositions from these samples can therefore be used to constrain the peak p–T conditions for the area.

The input rock composition of metapelitic granulite sample resulted from the projection of the actual rock composition (TK-12, Table 11) into the NCKFMASH system. The resulting isochemical section (Fig. 9a) predicts that melt coexists with garnet–biotite–K-feldspar–quartz in a p–T field around 800–1000 °C and at pressures between 5.4 kbar and 6.8 kbar.

Peak assemblage for the migmatite sample Tk-10 is inferred to contain garnet–biotite–K-feldspar–plagioclase–quartz–melt. The peak field in the computed isochemical section (Fig. 9b) overlaps with the garnet–biotite–K-feldspar–plagioclase–melt–quartz univariant field. The overlapping p–T space defines peak metamorphic conditions for the migmatite sample are 620–850 °C at $p = \sim4$ to >11 kbar. Overall, the sequence of assemblages predicted by the isochemical sections is in good agreement with those observed in rock sections in the metapelites and migmatites.

The peak metamorphic conditions for the sapphirine–orthopyroxene–cordierite–melt assemblage in the fine-grained sample P-63 is defined by the p–T space at $p \geq 8.4$ kbar at T 900 °C in the isochemical section (Fig. 9c). The absence of spinel-bearing assemblage in this sample constrains the peak T to <1000 °C. The calculated isochemical section (Fig. 9c) predicts a stability field for the assemblage sapphirine–orthopyroxene–cordierite. In sample P-60, the computed isochemical section (Fig. 9d) predicts a stability field for the sapphirine–orthopyroxene–sillimanite–K-feldspar assemblage at pressures between 6.8 and 8.2 kbar in a broad thermal domain from 900 to 1000 °C.

The calculated isochemical section (Fig. 9e) predicts a stability field for the biotite–sapphirine–orthopyroxene–cordierite–melt assemblage together with plagioclase and K-feldspar in coarse-grained sample P-61 at pressures around 8.2 kbar in a narrow

Table 11   Whole rock analyses (molar percent) of metapelites and sapphirine granulites.

Sample	TK-12	TK-10	P-63	P-61	P-60
SiO_2	66.54	62.79	43.41	57.57	43.17
Al_2O_3	12.54	7.69	12.17	17.26	16.57
FeO	6.65	10.56	4.98	2.84	6.76
MgO	3.46	10.19	29.53	14.68	28.92
CaO	0.77	1.13	0.83	0.6	0.6
Na_2O	1.54	0.86	0.81	0.16	0.46
K_2O	4.35	3.08	4.73	5.47	2.14
H_2O	4.15	3.69	3.54	1.42	1.38

Note: the unit of the oxides is %.

thermal domain around 850–950 °C. Considering the probable melt-bearing origin of the K-feldspar rims on plagioclase, this seems a reasonable reproduction of the assemblage actually observed in the studied rock.

The retrograde history of the rocks can be considered in the context of the estimated peak conditions. In the case of the Si-saturated metapelites, reaction microstructures are limited. The metapelites were particularly mineralogically insensitive to changes in p or T from peak conditions, as corroborated by the large p–T extent of peak assemblage fields across which there are very small (<5 mol%) changes in mineral modal abundances. The migmatites show some reaction microstructures but as they are influenced by local domainal chemistry, they cannot be confidently represented by the calculated isochemical sections. The post-peak metamorphic evolution is constrained by microstructures preserved in garnet-bearing sapphirine granulites. The development of narrow cordierite coronae on Opx–Spr symplectites is consistent with a decompressive cooling path. The post-peak p–T trajectory for the Panasapattu is also consistent with the development of cordierite rims around garnet, and the growth of retrograde biotite in metapelites.

7. Discussion

The stable coexistence of sapphirine and quartz and the occurrence of the assemblage high alumina orthopyroxene + sillimanite + quartz in the samples investigated in this study provide robust evidence for extreme crustal metamorphism at ultrahigh temperatures in this locality. The highest $w(Al_2O_3)$ content (9.86%) of these orthopyroxenes falls within the range of the orthopyroxenes of the Forefinger Point metamorphic belt in Enderby Land, Antarctica ($w(Al_2O_3) = 8\%$–9.5% occurring in the orthopyroxene + sillimanite + garnet + quartz rocks) where Harley et al. (1990) estimated metamorphic p–T conditions of 10 ± 1.5 kbar and 950 ± 50 °C. Likewise, high $w(Al_2O_3)$ orthopyroxenes have been reported from other UHT belts with values comparable to those observed in this study, such as the UHT granulites of Ganguvarpatti (8.5%–9.4%, Tamashiro et al., 2004) and Rajapalaiyam (8.5%–9.7%, Tateishi et al., 2004) in India and from the UHT belt in the northern margin of North China Craton (Santosh et al., 2007, 2009b) which all show metamorphic temperatures in excess of 1000 °C. The temperatures computed from conventional geothermometers indicate that the peak metamorphism took place at 970 °C within the realm of UHT. However, the stability relations of some of the assemblages observed in this study indicate that the peak metamorphic temperatures were probably much higher than this estimate. For example, the available phase equilibrium data suggest that sapphirine + quartz is stable at $T > 1030$ °C at 9.5 kbar (Hensen and Green, 1973) or $T > 1050$ °C at 11 kbar (Bertrand et al., 1991). Recent thermodynamic calculations in the KFMASH system also support the high-temperature nature of this assemblage ($T > 1005$ °C, Kelsey et al., 2004; Kelsey, 2008). An assemblage of sapphirine + quartz similar to that reported in this study has also been documented from other granulite terrains where it is taken as a key evidence for Peak UHT metamorphism at $T > 1000$ °C. Sapphirine in equilibrium with quartz was reported from quartzo-felspathic and pelitic granulites from the southern part of the Madurai Block around Rajapalaiyam in southern India by Tateishi et al. (2004). In Rajapalaiyam, however, the assemblage is preserved only as rare inclusions in the core of coarse-grained sub-hedral garnet. Sapphirine + quartz stable assemblage was also

reported recently from UHT rocks in the Cambrian collisional of Gondwana in southern India (Nishimiya et al., 2010). Sapphirine + quartz occurrences have also been recorded from other terranes including In Ouzzal (Ouzegane and Boumaza, 1996) and the Highland Complex (Yoshimura et al., 2008). When compared with the rare occurrence of sapphirine + quartz assemblages as minor inclusions in other minerals within UHT rocks as reported in the published literature, the common occurrence of sapphirine + quartz in the matrix of Mg−Al granulites from Panasapattu locality clearly indicates their stability during peak metamorphic conditions. The calculated Fe^{3+} of the sapphirines analyzed in this study is low, less than 0.27 p.f.u., and therefore meet the criteria as an indicator for UHT metamorphism (see Harley, 2008). It is therefore inferred that the peak UHT metamorphism of the Mg−Al granulites in the granulite belt in Panasapattu occurred at temperatures in excess of 1000 °C and pressures greater than 10 kbar.

In the KFMASH system, sapphirine + silicate melt can coexist above approximately 900 °C (Kelsey et al., 2005) implying that the sapphirine assemblages along with the co-spatial magnesian metapelitic granulites are melt-bearing UHT assemblages. Using isochemical sections in the NCKFMASH model system, White et al. (2001) and White and Powell (2002) have demonstrated that in a closed system (i.e., one from which no melt was lost), granulite facies mineral assemblages coexist with melt. To avoid complete retrogression, some melt loss or separation from residual mineral assemblages must occur (e.g., Powell and Downes, 1990; Kriegsman, 2001; Brown, 2002; White and Powell, 2002). In the case of melt segregation rather than loss, the retrogression depends on the size of the equilibration volume (Stüwe, 1997), which decreases with falling temperature. Segregation followed by melt loss is common in granulites, consistent with depleted bulk compositions (Fyfe, 1973) and residual mineral assemblages and microstructures that mimic melt-solid relations (Sawyer, 2001). On the basis of the isochemical sections of White and Powell (2002), a loss of 80 vol.% of the melt generated from an aluminous metapelite is necessary to preserve a granulite facies mineral assemblage, although such a mineral assemblage can be preserved with only 40% melt loss in a sub-aluminous metapelite.

The present study documents unequivocal presence of Spr + Qtz from UHT granulites from the south-central sector of the Eastern Ghats belt. The presence of Spr + Qtz in granulites is rarely documented from the Eastern Ghats belt particularly as a stable matrix mineral assemblage. Detailed studies of the granulite facies metamorphic belts in different domains of the Eastern Ghats belt, probably formed during different stages of exhumation in a protracted subduction−accretion regime would provide more insights on the formation of extreme metamorphic orogens in this major collisional belt. The documentation of such UHT granulite belts is crucial to characterize the fertility of crustal source in the protracted evolution of the Eastern Ghats belt.

8. Concluding remarks

Coexisting sapphirine + quartz in equilibrium within biotite−garnet−orthopyroxene−sillimanite granulites from Paderu complex demonstrates that UHT metamorphic conditions were achieved in this terrane. The minimum conditions estimated for the metamorphic peak in this study are around 1030−1050 °C. The metapelites from the Paderu terrane provide strong evidence of dehydration melting of biotite in the UHT field. Isochemical

sections constructed in the NCKFMASH system and contoured for modal proportions of melt and garnet, and for compositional isopleths of garnet, adequately predict phase and reaction relations that are consistent with those observed in the rocks. These isochemical sections offer additional constraints on the $p−T−x$ evolution which could not be tapped from conventional thermobarometric computations. The generally migmatitic aspect of the high-grade metapelites confirms that these rocks were melt-bearing, although no major melt loss is indicated. The down-temperature reaction with residual melt may partially to completely overprint the evidence for the peak UHT metamorphic history, and therefore, the non-UHT domains may represent the retrograded equivalents.

The UHT decompressional $p−T$ history deduced from Panasapattu metapelitic sapphirine granulite is comparable to several Grt−Opx−Sill occurrences worldwide (Harley, 1998a, b and references therein). High-temperature decompression followed by cooling for metapelitic granulites has also been described from other parts of the Eastern Ghats such as Ankapalle (Dasgupta et al., 1994), Chilka Lake (Sen et al., 1995), Sunkarametta (Bose et al., 2000), and Pangidi (Dharma Rao, 1998, 2000). Although precise geochronological data are not available for the present study area, the timing of UHT metamorphism in the Eastern Ghats granulite belt from UHT rocks in different localities (e.g., Upadhyay et al., 2009; Das et al., 2010) shows a range of ages from early Mesoproterozoic to Neoproterozoic, suggesting multiple metamorphic events of passive margin sediments and oceanic components during the ca. 500 Ma subduction−accretion history along this collisional belt. This inference is also supported by evidence from imbricated ocean plate stratigraphic sequences including ophiolite mélange occurring in the western margin of belt, with age of 1.33 Ga (Dharma Rao et al., 2010).

Models on extreme metamorphism in continental collisional belts take into account the thinning and later cooling of crust previously over-thickened by the collisional event (Thompson and England, 1984). Harley (1989) suggested that the granulites showing a decompression history followed by near isobaric cooling may develop in the later stages of the thermal evolution of over-thickened continental crust. The preservation of early deformation structures in aluminous sapphirine granulites, together with the record of ultrahigh-temperature decompression preceding isobaric cooling, is consistent with a clockwise $p−T$ path usually recorded from continental collisional belts, with the high temperature melting producing metapelitic sapphirine granulites probably suggesting the prograde segment.

Clockwise and counterclockwise $p−T$ paths are generally determined on the basis of the nature of the prograde path, and often, the prograde history of high-grade metamorphic rocks is obliterated by later processes including Barrovian hydration which commonly manifests in major orogens. Sometimes it is possible to have isobaric cooling and isothermal decompression retrograde trajectories associated with both clockwise and counterclockwise loops. Dasgupta et al. (1994) recorded decompression from granulites of Anakapalle in the Eastern Ghats belt of India that is characterized by counterclockwise $p−T$ path. Tsunogae et al. (2002) reported counterclockwise paths from UHT rocks in the Archean Napier Complex of Antarctica, and Santosh et al. (2007, 2009b) recorded counterclockwise $p−T$ trajectory from an ultra-hot orogen in the northern part of North China Craton. Recent analyses of $p−T$ paths in different metamorphic orogens (e.g., Masago et al., 2009, 2010; Maruyama et al., 2010) suggest that in many cases, the $p−T$ trajectories follow the model subduction geotherm, and a tectonic model in

which the metamorphic rocks are subducted and exhumed along a plate boundary is the most preferred model. In many metamorphic belts, the peak metamorphic conditions, particularly pressure, may have been underestimated because of a strong retrograde overprint. Santosh and Kusky (2010) recently proposed an alternate model for the generation of extreme metamorphic rocks associated with sub-duction−collision tectonics during continental amalgamation which suggests that the anomalous heat (and CO_2-rich volatile, e.g., Santosh and Omori, 2008a, b) input required to stabilize the 'dry' mineral assemblages within many of the reported UHT occurrences from collisional belts may be related to asthenospheric upwelling through slab window generated by ridge subduction. This model also accounts for the relatively lower pressures at extreme temperatures recorded from many UHT belts, as in the present case. The tectonic setting of the present area, within a subduction−accretion−collision belt, with associated arc magmatic units and imbricated ocean plate stratigraphy is in favor of such a model. Moreover, the wide range of ages reported for UHT metamorphism in this belt also attest to a prolonged history of convergent margin tectonics culminating in final collisional assembly. Further detailed work, particularly focusing on inclusion minerals and precise isotope geochronology may help unravel the mechanisms and timings of formation of UHT metamorphic belts within this collisional suture.

Acknowledgments

References

Aranovich, L.Y., 1984. Biotite-garnet equilibria in metapelites: II. Calculation of T, P and water fugacity. Contributions to Physico-Chemical Petrology 12, 92−103 (in Russian).

Aranovich, L.Y., Berman, R.G., 1996. Optimized standard state and solution properties of minerals. II. Comparisons, predictions, and applications. Contributions to Mineralogy and Petrology 126, 25−37.

Bertrand, P., Ellis, D.J., Green, D.H., 1991. The stability of sapphirine quartz and hypersthene-sillimanite-quartz assemblages: an experimental investigation in the system FeO−MgO−Al$_2$O$_3$−SiO$_2$ under H$_2$O and CO$_2$ conditions. Contributions to Mineralogy and Petrology 108, 55−71.

Bhattacharya, A., Krishnapur, K.R., Raith, M., Sen, S.K., 1991. An improved set of a−X parameters for Fe−Mg−Ca garnets and refinements of the ortho-pyroxene−garnet thermometer and the orthopyroxene−garnet−plagioclase−quartz barometer. Journal of Petrology 32, 629−656.

Bhattacharya, S., Kar, R., 2002. High-temperature dehydration melting and decompressive P−T path in a granulite complex from the Eastern Ghats, India. Contributions to Mineralogy and Petrology 143, 175−191.

Bhattacharya, S., Kar, R., Teixeira, W., Basei, M., 2003. High-temperature crustal anatexis in a clockwise P−T path: isotopic evidence from a granulite-granitoid suite in the Eastern Ghats belt, India. Journal Geological Society of London 160, 39−46.

Bose, S., Fukuoka, M., Sengupta, P., Dasgupta, S., 2000. Evolution of high-Mg−Al granulites from Sunkarametta, Eastern Ghats, India: evidence for a lower crustal heating-cooling trajectory. Journal of Metamorphic Geology 18, 223−240.

Brey, G.P., Kohler, T., 1990. Geothermobarometry in four-phase lherzo-lites. New thermobarometers, and practical assessment of existing thermobarometers. Journal of Petrology 3l, 1353−1378.

Brown, M., 2002. Retrograde processes in migmatites and granulites revisited. Journal of Metamorphic Geology 20, 25−40.

Brown, M., 2007. Metamorphic conditions in orogenic belts: a record of secular change. International Geology Review 49, 193−234.

Connolly, J.A.D., 2005. Computation of phase equilibria by linear programming: a tool for geodynamic modeling and its application to subduction zone decarbonation. Earth Planetary Science Letters 236, 524−541.

Das, K., Bose, S., Karmakar, S., Dunkley, D.J., Dasgupta, S., 2011. Multiple tectonometamorphic imprints in the lower crust: first evidence of ca. 950 Ma (zircon U-Pb SHRIMP) compressional reworking of UHT aluminous granulites from the Eastern Ghats Belt, India. Geological Journal 46, 217−239. doi:10.1002/gj.1246.

Das, K., Fujino, K., Tomioka, N., Miura, H., 2006. Experimental data on Fe and Mg partitioning between coexisting sapphirine and spinel: an empirical geothermometer and its application. European Journal of Mineralogy 18, 49−58.

Das, K., Dasgupta, S.H., Miura, H., 2010. An experimentally constrained petrogenetic grid in the silica-saturated portion of the system KFMASH at high temperatures and pressures. Journal of Petrology 44, 1055−1075.

Dasgupta, S., Sanyal, S., Sengupta, P., Fukuoka, M., 1994. Petrology of granulites from Anakapalle − evidence for Proterozoic decompression in the Eastern Ghats, India. Journal of Petrology 35, 433−459.

Dasgupta, S., Sengupta, P., 2003. Indo-Antarctic correlation: a perspective from the Eastern Ghats Belt. In: Yoshida, M., Windley, B.F., Dasgupta, S. (Eds.), Proterozoic East Gondwana: supercontinent assembly and breakup. Journal Geological Society of London 206, 131−143.

Dasgupta, S., Sengupta, P., Ehl, J., Raith, M., Bardhan, S., 1995. Reaction textures in a suite of spinel granulites from the Eastern Ghats Belt, India: evidence for polymetamorphism, a partial petrogenetic grid in the system KFMASH and the roles of ZnO and Fe$_2$O$_3$. Journal of Petrology 36, 435−461.

Dharma Rao, C.V., 1998. Petrological evolution of the Pangidi granulites, Eastern Ghats, India: evidence for decompressive and cooling retrograde trajectories. Neues Jahrbuch fur Mineralogie Abhandlungen 173, 305−326.

Dharma Rao, C.V., 2000. Metapelitic migmatites from Pangidi granulite complex, Eastern Ghats Belt, India: petrological constraints on crustal melting and tectonic exhumation. Gondwana Research 3, 105−117.

Dharma Rao, C.V., Chmielowski, R., 2010. New constraints on the metamorphic evolution of the Eastern Ghats Belt, India, based on relict sapphirine-spinel inclusions in garnet from ultra high temperature granulites. Geological Journal 46, 240−262.

Dharma Rao, C.V., Reddy, U.V.B., 2009. Petrological and geochemical characterization of ophiolite mélange, Nellore-Khammam schist belt, SE India. Journal of Asian Earth Sciences 65, 261−276.

Dharma Rao, C.V., Santosh, M., 2011. Continental arc magmatism in a Mesoproterozoic convergent margin: petrological and geochemical constraints from the Pangidi − Kondapalle complex along the eastern margin of the Indian plate. Tectonophysics. doi:10.1016/j.tecto.2011.06.025.

Dharma Rao, C.V., Santosh, M., Dong, Y.P., 2011a. LA-ICP-MS U-Pb age data of anorthosites from Pangidi − Kondapalle Layered Intrusion, Eastern Ghats belt, India: constraints on Mesoproterozoic magmatism in a convergent margin setting. Journal of Asian Earth Sciences. doi: 10.1016/j.jseaes.2011.07.005.

Dharma Rao, C.V., Santosh, M., Wu, Y.B., 2011b. Mesoproterozoic ophiolitic melange from the SE periphery of the Indian plate: U-Pb zircon ages and tectonic implications. Gondwana Research 19, 384−401.

Dharma Rao, C.V., Windley, B.F., Choudhary, A.K., 2010. The Chimalpahad anorthosite complex and associated basaltic amphibolites, Nellore Schist Belt, India: magma chamber and roof of a Proterozoic island arc. Journal of Asian Earth Sciences 40 (5), 1027−1043.

Dobmeier, C.J., Raith, M.M., 2003. Crustal architecture and evolution of the Eastern Ghats Belt and adjacent regions of India. Journal Geological Society of London 206, 145−168.

Eckert Jr., J.O., Newton, R.C., Kleppa, O.J., 1991. The ΔH of reaction and recalibration of garnet-pyroxene-plagioclase-quartz geobarometers in

the CMAS system by solution calorimetry. American Mineralogist 76, 148–160.

Fitzsimons, I.C.W., Harley, S.L., 1994. The influence of retrograde cation exchange on granulite $P–T$ estimates and convergence technique for the recovery of peak metamorphic conditions. Journal of Petrology 35, 543–576.

French, J.E., Heaman, L.M., Chacko, T., Srivastava, R.K., 2008. 1891–1883 Ma Southern Bastar–Cuddapah mafic igneous events, India: a newly recognized large igneous province. Precambrian Research 160, 308–322.

Fyfe, W.S., 1973. The granulite facies, partial melting and the Archaean crust. Philosophical Transactions of Royal Society of London 273, 457–461.

Gupta, S., 2004. The Eastern Ghats Belt, India — a new look at an old orogen. Geological Survey of India Special Publications 84, 75–100.

Harley, S.L., 1984a. An experimental study of the partitioning of Fe and Mg between garnet and orthopyroxene. Contributions to Mineralogy and Petrology 86, 359–373.

Harley, S.L., 1984b. The solubility of alumina in orthopyroxene coexisting with garnet in FeO–MgO–Al$_2$O$_3$–SiO$_2$, and CaO–FeO–MgO–Al$_2$O$_3$–SiO$_2$. Journal of Petrology 25, 665–696.

Harley, S.L., 1985. Garnet–orthopyroxene-bearing granulites from Enderby Land, Antarctica: metamorphic pressure–temperature–time evolution of the Archaean Napier Complex. Journal of Petrology 26, 819–856.

Harley, S.L., 1989. The origins of granulites: a metamorphic perspective. Geological Magazine 126, 215–247.

Harley, S.L., 1998a. On the occurrence and characterization of ultrahigh-temperature crustal metamorphism. In: Treloar, P.J., O'Brien, P.J. (Eds.), What Drives Metamorphism and Metamorphic Reactions?. Geological Society of London Special Publications 138, 81–107.

Harley, S.L., 1998b. An appraisal of peak temperatures and thermal histories in ultrahigh-temperature (UHT) crustal metamorphism: the significance of aluminous orthopyroxene. Memoirs of National Institute of Polar Research, Special Issue 53, 49–73.

Harley, S.L., 2008. Refining the $P–T$ records of UHT crustal metamorphism. Journal of Metamorphic Geology 26, 125–154.

Harley, S.L., Hensen, B.J., Sheraton, J.W., 1990. Two-stage decompression in orthopyroxene–sillimanite granulites from Forefinger Point, Enderby Land, Antarctica: implications for the evolution of the Archaean Napier Complex. Journal of Metamorphic Geology 8, 591–613.

Harley, S.L., Motoyoshi, Y., 2000. Al zoning in orthopyroxene in sapphirine quartzite: evidence for >1120 °C UHT metamorphism in the Napier Complex, Antarctica, and implications for the entropy of sapphirine. Contributions to Mineralogy and Petrology 138, 293–307.

Hensen, B.J., Green, D.H., 1973. Experimental study of the stability of cordierite and garnet in pelitic compositions at high pressures and temperatures. III. Synthesis of experimental data and geological applications. Contributions to Mineralogy and Petrology 38, 151–166.

Holland, T.J.B., Powell, R., 1996. Thermodynamics of order-disorder in minerals 1: symmetric formalism applied to minerals of fixed composition. American Mineralogist 81, 1413–1424.

Holland, T.J.B., Powell, R., 1998. An internally-consistent thermodynamic dataset for phases of petrological interest. Journal of Metamorphic Geology 16, 309–344.

Holland, T.J.B., Powell, R., 2001. Calculation of phase relations involving haplogranitic melts using an internally-consistent thermodynamic data set. Journal of Petrology 42, 673–683.

Isozaki, Y., Aoki, K., Nakama, T., Yanai, S., 2010. New insight into a subduction-related orogen: a reappraisal of the geotectonic framework and evolution of the Japanese Islands. Gondwana Research 18, 82–105.

Kawasaki, T., Matsui, Y., 1983. Thermodynamic analysis of equilibria involving olivine, orthopyroxene and garnet. Geochimica et Cosmochimica Acta 47, 1661–1680.

Kelsey, D.E., 2008. On ultra-high temperature crustal metamorphism. Gondwana Research 13, 1–29.

Kelsey, D.E., White, R.W., Holland, T.J.B., Powell, R., 2004. Calculated phase equilibria in K$_2$O–FeO–MgO–Al$_2$O$_3$–SiO$_2$–H$_2$O for

sapphirine–quartz-bearing mineral assemblages. Journal of Metamorphic Geology 22, 559–578.

Kelsey, D.E., White, R.W., Holland, T.J.B., Powell, R., 2005. Calculated phase equilibria in K$_2$O–FeO–MgO–Al$_2$O$_3$–SiO$_2$–H$_2$O for silica-undersaturated sapphirine-bearing mineral assemblages. Journal of Metamorphic Geology 23, 217–239.

Kerrick, D.M., Jacobs, G.K., 1981. A modified Redlich–Kwong equation of state for H$_2$O, CO$_2$, and H$_2$O–CO$_2$ mixtures at elevated pressures and temperatures. American Journal of Science 281, 735–767.

Kriegsman, L.M., 2001. Partial melting, partial melting extraction and partial back reaction in anatectic migmatites. Lithos 56, 75–96.

Lal, R.K., 1993. Internally consistent recalibrations of mineral equilibria for geothermobarometry involving garnet-plagioclase-quartz assemblages and their applications to the south Indian granulites. Journal of Metamorphic Geology 11, 855–866.

Lal, R.K., 2003. Metamorphic evolution of granulites from southern Indian shield. Geological Society of India Memoir 52, 61–108.

Lal, R.K., Ackermand, D., Upadhyay, H., 1987. $P–T–X$ relationships deduced from corona textures in sapphirine spinel quartz assemblages from Paderu, South India. Journal of Petrology 28, 1139–1168.

Lavrent'eva, L.V., Perchuk, L.L., 1990. Orthopyroxene–garnet geothermometer: experiments and theoretical treatment of data base. Doklady Akademi Nauk SSR 260, 731–734.

Lee, H.Y., Ganguly, J., 1988. Equilibrium compositions of coexisting garnet and orthopyroxene: reversed experimental determinations in the system FeO–MgO–Al$_2$O$_3$–SiO$_2$, and applications. Journal of Petrology 29, 93–98.

Maruyama, S., Masago, H., Katayama, I., Iwase, Y., Toriumi, M., Omori, S., Aoki, K., 2010. A new perspective on metamorphism and metamorphic belts. Gondwana Research 18, 106–137.

Masago, H., Omori, S., Maruyama, S., 2009. Counter-clockwise prograde $P–T$ path in collisional orogeny and water subduction at the Precambrian–Cambrian boundary: the ultrahigh-pressure pelitic schist in the Kokchetav massif, northern Kazakhstan. Gondwana Research 15, 137–150.

Masago, H., Omori, S., Maruyama, S., 2010. Significance of retrograde hydration in collisional metamorphism: a case study of water infiltration in the Kokchetav ultra-high pressure metamorphic rocks, northern Kazakhstan. Gondwana Research 18 (1), 205–212.

Moecher, D.P., Essene, E.,J., Anovitz, L.M., 1988. Calculation and application of clinopyroxene-garnet-plagioclase-quartz geobarometers. Contributions to Mineralogy and Petrology 100, 92–106.

Mohan, A., Tripathi, P., Motoyoshi, Y., 1997. Reaction history of sapphirine granulites and a decompressional $P–T$ path in a granulite complex from the Eastern Ghats. Proceedings of Indian Academy of Sciences (Earth Planetary Science) 106, 115–129.

Moraes, R., Brown, M., Fuck, R.A., Camargo, M.A., Lima, T.M., 2002. Characterization and $P–T$ evolution of melt-bearing ultrahigh-temperature granulites: an example from the Anápolis–Itauçu complex of the Brasília Fold Belt, Brazil. Journal of Petrology 43, 1673–1705.

Mukhopadhyay, D., Basak, K., 2009. The Eastern Ghats Belt. A polycyclic granulite terrain. Journal of the Geological Society of India 73, 489–518.

Nair, R., Chacko, T., 2002. Fluid-absent melting of high-grade semi-pelites: $P–T$ constraints on orthopyroxene formation and implications for granulite genesis. Journal of Petrology 43, 2121–2142.

Nasipuri, A., Bhattacharya, A.S., Das, S., 2009. Metamorphic reactions in dry and aluminous granulites: a Perple_X P–T pseudosection analysis of the influence of effective reaction volume. Contributions to Mineralogy and Petrology 157 (3), 301–311.

Nickel, K.G., Green, D.H., 1985. Empirical geothermobarometry for garnet peridotites and implications for the nature of the lithosphere, kimberlites and diamonds. Earth Planetary Science Letters 73, 158–170.

Nishimiya, Y., Tsunogae, T., Santosh, M., 2010. Sapphirine + quartz corona around magnesian (x_{Mg} ∼0.58) staurolite from the Palghat-Cauvery Suture Zone, southern India: evidence for high-pressure and ultrahigh-temperature metamorphism within the Gondwana suture. Lithos 114, 490–502.

Owen, J.V., Greenough, J.D., Fryer, B.J., 1991. The nature of sialic basement to the Dunnage zone, northern Newfoundland: evidence from crustal xenoliths. Canadian Journal of Earth Sciences 28 (7), 1073−1077.

Ouzegane, K., Boumaza, S., 1996. An example of ultra-high-temperature metamorphism: orthopyroxene-sillimanite-garnet, sapphirine-quartz and spinel-quartz parageneses in Al−Mg granulites from In Hihaou, In Ouzzal, Hoggar. Journal of Metamorphic Geology 14, 693−708.

Pal, S., Bose, S., 1997. Mineral reactions and geothermobarometry in a suite of granulite facies rocks from Paderu, Eastern Ghats granulite belt: a reappraisal of the P−T trajectory. Proceedings of Indian Academy of Sciences (Earth Planetary Sciences) 106, 77−89.

Pattison, D.R.M., Begin, N.J., 1994. Compositional maps of metamorphic orthopyroxene and garnet: evidence for a hierarchy of closure temperatures and implications for geothermometry of granulites. Journal of Metamorphic Geology 12, 387−410.

Pattison, D.R.M., Chacko, T., Farquhar, J., McFarlane, C.R.M., 2003. Temperatures of granulite-facies metamorphism: constraints from experimental phase equilibria and thermobarometry corrected for retrograde exchange. Journal of Petrology 44, 867−900.

Perchuk, L., Aranovich, L.Y., Podleskii, K.K., Lavrent'eva, I.V., Gerasimov, V.Y.U., Fedk'in, V.V., Kitsul, Y.I., Karsakov, L.P., Berdnikov, N.V., 1985. Precambrian granulites of the Aldan Shield, eastem Siberia, USSR. Journal of Metamorphic Geology 3, 265−310.

Perkins, D., Chipera, S.J., 1985. Gamet-orthopyroxene-plagioclase-quartz geobarometry: refinements and application to the English River sub-province and the Minnesota River Valley. Contributions to Mineralogy and Petrology 89, 69−80.

Perkins, D., Newton, R.C., 1981. Chamockite geobarometer based on coexisting garnet-pyroxene-plagioclase-quartz. Nature 292, 144−146.

Powell, R., Downes, J., 1990. Garnet porphyroblast-bearing leucosomes in metapelites: mechanisms, phase diagrams, and example from Broken Hill, Australia. In: Ashworth, J.R., Brown, M. (Eds.), High Temperature Metamorphism and Crustal Anatexis. Unwin Hyman, London, pp. 105−123.

Powell, R., Holland, T.J.B., 1999. Relating formulations of the thermodynamics of mineral solid solutions: activity modeling of pyroxenes, amphiboles, and micas. American Mineralogist 84 (1−2), 1−14.

Powell, M., Powell, R., 1977. Plagioclase-alkali feldspar geothermometry revisited. Mineralogical Magazine 41, 253−256.

Rickers, K., Mezger, K., Raith, M.M., 2001. Evolution of the continental crust in the Proterozoic Eastern Ghats Belt, India and new constraints for Rodinia reconstruction: implications from Sm−Nd, Rb−Sr and Pb−Pb isotopes. Precambrian Research 112, 183−210.

Rogers, J.J.W., Santosh, M., 2002. Configuration of Columbia, a Mesoproterozoic supercontinent. Gondwana Research 5, 5−22.

Rogers, J.J.W., Santosh, M., 2009. Tectonic and surface effects of the supercontinent Columbia. Gondwana Research 15, 373−380.

Saha, D., 2011. Dismembered ophiolites in Paleoproterozoic nappe complexes of Kandra and Gurramkonda, South India. Journal of Asian Earth Sciences 42 (3), 158−175.

Saha, L., Bhowmik, S.K., Fukuoka, M., Dasgupta, S., 2008. Contrasting episodes of regional granulite-facies metamorphism in enclaves and host gneisses from the Aravalli-Delhi mobile belt, NW India. Journal of Petrology 49, 107−128.

Santosh, M., 2010. Assembling North China Craton within the Columbia supercontinent: the role of double-sided subduction. Precambrian Research 178, 149−167.

Santosh, M., Kusky, T., 2010. Origin of paired high pressure−ultrahigh-temperature orogens: a ridge subduction and slab window model. Terra Nova 22, 35−42.

Santosh, M., Maruyama, S., Sato, K., 2009a. Anatomy of a Cambrian suture in Gondwana: Pacific-type orogeny in southern India? Gondwana Research 16, 321−341.

Santosh, M., Omori, S., 2008a. CO$_2$ flushing: a plate tectonic perspective. Gondwana Research 13, 86−102.

Santosh, M., Omori, S., 2008b. CO$_2$ windows from mantle to atmosphere: models on ultrahigh-temperature metamorphism and speculations on the link with melting of snowball Earth. Gondwana Research 14, 82−96.

Santosh, M., Sajeev, K., Li, J.H., Liu, S.J., Itaya, T., 2009b. Counterclockwise exhumation of a hot orogen: the Paleoproterozoic ultrahigh-temperature granulites in the North China Craton. Lithos 110, 140−152.

Santosh, M., Tsunogae, T., Li, J.H., Liu, S.J., 2007. Discovery of sapphirine-bearing Mg−Al granulites in the North China Craton: implications for Paleoproterozoic ultrahigh-temperature metamorphism. Gondwana Research 11, 263−285.

Santosh, M., Zhao, D., Kusky, T., 2010. Mantle dynamics of the Paleoproterozoic North China Craton: a perspective based on seismic tomography. Journal of Geodynamics 49, 39−53.

Sawyer, E.W., 2001. Melt segregation in the continental crust: distribution and movement of melt in anatectic rocks. Journal of Metamorphic Geology 19, 291−309.

Schreyer, W.V., Maresch, P., Daniels, P., Wolfsdorff, P., 1990. Potassic cordierites: characteristic minerals for high-temperature, very low-pressure environments. Contributions to Mineralogy and Petrology 105, 162−172.

Sen, S.K., Bhattacharya, A., 1984. An orthopyroxene-garnet thermometer and its application to the Madras charnockites. Contributions to Mineralogy and Petrology 88, 64−71.

Sen, S.K., Bhattacharya, S., Acharya, A., 1995. A multi-stage pressure-temperature record in the Chilka Lake epitome of the metamorphic evolution of Eastern Ghats, India? Journal of Metamorphic Geology 14, 287−298.

Sengupta, P., Dasgupta, S., Bhattacharya, P.K., Fukuoka, M., Chakraborti, S., Bhowmick, S., 1990. Petro-tectonic imprints in the sapphirine granulites from Anantagiri, Eastern Ghats Mobile Belt, India. Journal of Petrology 31, 971−996.

Sengupta, P., Dasgupta, S., Ehl, J., Raith, M.M., 1997. Thermobaric evolution of a suite of Mg−Al granulites from Paderu: further evidence for a ACW P−T path in the Eastern Ghats Belt, India. European Journal of Mineralogy, 331−342.

Sengupta, P., Raith, M.M., DasGupta, S., 2004. Comment on: 'High-temperature dehydration melting and decompressive P−T path in a granulite complex from the Eastern Ghats India' by S. Bhattacharya and R. Kar. Contributions to Mineralogy and Petrology 147, 123−125.

Sengupta, P., Sen, J., Dasgupta, S., Raith, M., Bhui, K., Ehl, J., 1999. Ultrahigh temperature metamorphism of metapelitic granulites from Kondapalle, Eastern Ghats Belt: implications for the Indo-Antarctic correlation. Journal of Petrology 40, 1065−1087.

Simmat, R., Raith, M.M., 2008. U−Th−Pb monazite geochronometry of the Eastern Ghats Belt, India: timing and spatial disposition of poly-metamorphism. Precambrian Research 162, 16−39.

Stormer Jr., J.C., 1975. A practical two-feldspar geothermometer. American Mineralogist 60, 667−674.

Stormer Jr., J.C., Whitney, J.A., 1985. Two feldspar and iron−titanium oxide equilibria in silicic magmas and the depth of origin of large volume ash-flow tuffs. American Mineralogist 70, 52−64.

Stüwe, K., 1997. Effective bulk composition changes due to cooling: a model predicting complexities in retrograde reaction textures. Contributions to Mineralogy and Petrology 129, 43−52.

Tamashiro, I., Santosh, M., Morimoto, T., Tsunogae, T., 2004. High alumina orthopyroxenes from Ganguvarpatti granulites, southern India: implications for ultrahigh-temperature metamorphism. Journal of Mineralogy and Petrology Sciences 99, 279−297.

Tateishi, K., Tsunogae, T., Santosh, M., Janardhan, A.S., 2004. First report of sapphirine + quartz assemblage from southern India: implications for ultrahigh-temperature metamorphism. Gondwana Research 7, 899−912.

Thompson, A.B., England, P.C., 1984. Pressure−temperature−time paths of regional metamorphism II. Their inference and interpretation using mineral assemblages in metamorphic rocks. Journal of Petrology 25, 929−955.

Thompson Jr., J.B., Hovis, G.L., 1979. Entropy of mixing in sanidine. American Mineralogist 64, 57−65.

Tinkham, D.K., Zuluaga, C.A., Stowell, H.H., 2001. Metapelite phase equilibria modeling in MnNCKFMASH: the effect of variable Al$_2$O$_3$ and MgO/(MgO + FeO) on mineral stability. Geological Materials Research 3, 1−42.

Tsunogae, T., Santosh, M., Osanai, Y., Owada, M., Toyoshima, T., Hokada, T., 2002. Very high-density carbonic fluid inclusions in sapphirine-bearing granulites from Tonagh Island in the Archean Napier Complex, East Antarctica: implications for CO_2 infiltration during ultrahigh-temperature (T > 1, 100 °C) metamorphism. Contributions to Mineralogy and Petrology 143, 279–299.

Upadhyay, D., Gerdes, A., Raith, M.M., 2009. Unraveling sedimentary provenance and tectono-thermal history of high temperature metapelites using zircon and monazite chemistry: a case study from the Eastern Ghats Belt, India. Journal of Geology 117, 665–683.

Vielzeuf, D., Montel, J.M., 1994. Partial melting of metagreywackes Part I. Fluid-absent experiments and phase relationships. Contributions to Mineralogy and Petrology 117, 375–393.

Vry, J.K., Brown, P.E., Valley, J.W., 1990. Cordierite volatile content and the role of CO_2 in high-grade metamorphism. American Mineralogist 75, 71–88.

White, R.W., Powell, R., 2002. Melt loss and the preservation of granulite facies mineral assemblages. Journal of Metamorphic Geology 20, 621–632.

White, R.W., Powell, R., Holland, T.J.B., 2001. Calculation of partial melting equilibria in the system $Na_2O–CaO–K_2O–FeO–MgO–Al_2O_3–SiO_2–H_2O$ (NCKFMASH). Journal of Metamorphic Geology 19, 139–153.

Whitney, D.L., Evans, B.W., 2010. Abbreviations for names of rock-forming minerals. American Mineralogist 95, 185–187.

Yoshimura, Y., Motoyoshi, Y., Miyamoto, T., 2008. Sapphirine + quartz association in garnet: implication for ultrahigh-temperature metamorphism at Rundvagshetta, Lutzow-Holm Complex, East Antarctica. The Geological Society of London, Special Publications 308, 377–390.

Zeh, A., Holness, M., 2003. The effect of reaction overstep on garnet microtextures in metapelitic rocks of the Ilesha Schist Belt, SW Nigeria. Journal of Petrology 44, 967–994.